

AD-A058 690

CHARLES STARK DRAPER LAB INC CAMBRIDGE MA
MATERIALS RESEARCH FOR ADVANCED INERTIAL INSTRUMENTATION. TASK --ETC(U)
JUL 78 D DAS, E WETTSTEIN, K KUMAR

F/G 20/3

N00014-77-C-0388

UNCLASSIFIED

R-1177

NL

| OF |

AD
A058 690



END
DATE
FILMED
11-78

DDC

AD A0 58690

DDC FILE COPY

LEVEL II

12
Sc

R-1177

6

**MATERIALS RESEARCH FOR ADVANCED
INERTIAL INSTRUMENTATION.**

**TASK 3. RARE EARTH MAGNETIC MATERIAL
TECHNOLOGY AS RELATED TO
GYRO TORQUERS AND MOTORS.**

9

**TECHNICAL REPORT NO. 1,
FOR THE PERIOD
31 SEPTEMBER 1977 - 31 JUNE 1978.**

10

By
D. DAS, E. WETTSTEIN, K. KUMAR

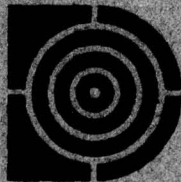
15

Prepared for the Office of Naval Research,
Department of the Navy, Under Contract
N00014-77-C-0388

DDC
SEP 14 1978
F

Approved for Public Release; Distribution Unlimited.
Permission is Granted the U.S. Government to
Reproduce This Paper in Whole Or in Part.

11, Jul 78



12 66p.

The Charles Stark Draper Laboratory, Inc.
Cambridge, Massachusetts 02139

78 09 07 001
408 386
LB

REPORT DOCUMENTATION PAGE		READ INSTRUCTIONS BEFORE COMPLETING FORM
1. REPORT NUMBER TECHNICAL REPORT NO. 1 ✓	2. GOVT ACCESSION NO.	3. RECIPIENT'S CATALOG NUMBER
4. TITLE (and Subtitle) MATERIALS RESEARCH FOR ADVANCED INERTIAL INSTRUMENTATION TASK 3: RARE EARTH MAGNETIC MATERIAL TECHNOLOGY AS RELATED TO GYRO TORQUERS AND MOTORS	5. TYPE OF REPORT & PERIOD COVERED Research Report 9/30/77 - 6/30/78	
	6. PERFORMING ORG. REPORT NUMBER R-1177 ✓	
7. AUTHOR(s) D. Das, E. Wettstein, and K. Kumar	8. CONTRACT OR GRANT NUMBER(s) N-00014-77-C-0388 ^{new}	
9. PERFORMING ORGANIZATION NAME AND ADDRESS The Charles Stark Draper Laboratory, Inc./ 555 Technology Square, Cambridge, Massachusetts 02139		10. PROGRAM ELEMENT, PROJECT, TASK AREA & WORK UNIT NUMBERS
11. CONTROLLING OFFICE NAME AND ADDRESS Office of Naval Research Department of the Navy 800 N. Quincy Street, Arlington, Virginia 22217	12. REPORT DATE July 1978	
	13. NUMBER OF PAGES 72	
14. MONITORING AGENCY NAME & ADDRESS (if different from Controlling Office) Office of Naval Research - Boston Branch 666 Summer Street Boston, Massachusetts 02210	15. SECURITY CLASS. (of this report) Unclassified	
	15a. DECLASSIFICATION/DOWNGRADING SCHEDULE	
16. DISTRIBUTION STATEMENT (of this Report) <div style="border: 1px solid black; padding: 5px; width: fit-content; margin: 10px auto;">This document has been approved for public release and sale; its distribution is unlimited.</div>		
17. DISTRIBUTION STATEMENT (of the abstract entered in Block 20, if different from Report)		
18. SUPPLEMENTARY NOTES		
19. KEY WORDS (Continue on reverse side if necessary and identify by block number) Coercivity Stability Hot Isostatic Pressing Stability Measurements Magnet Temperature Compensation Samarium-Cobalt Sintering		
20. ABSTRACT (Continue on reverse side if necessary and identify by block number) For inertial applications aligned SmCo ₅ magnets with high flux stability, close-to-zero reversible temperature coefficient of magnetization, and a thermal expansion similar to that of beryllium are required. High flux stability is being attempted by producing high H _{c1} (high resistance to demagnetization) and high H _{c2} (high second quadrant loop squareness) magnets through the attainment of fine grain size, low oxygen content and high density in the material. Low reversible temperature coefficient will be achieved by suitable samarium replacement with a heavier rare earth element while the thermal expansion coefficient will be tailored (to that of beryllium) by controlling the alignment of the crystals in the magnet. ↘		

(continued on next page)

20. ABSTRACT

In line with these requirements a magnet sintering facility capable of ultra-high vacuum operation (10^{-6} torr capability at 1100°C) has been fabricated for oxygen-free processing of these magnets. Techniques for producing powder with low oxygen contamination (from the environment) have also been developed for this purpose. The total amount of oxygen incorporated into the powder is found to be considerably less than what is obtained with conventional procedures. This has resulted in remarkably high values of H_c and H_k in sintered SmCo_5 magnets produced so far. An unprecedented value of 29 kOe has been measured for H_c in a few of the magnets as compared to 5 to 10 kOe found in most commercial magnets. The energy product values of these magnets have been limited to about 13 mGOe because of poor alignment. Investigations currently in progress are expected to result in substantial improvements in the values of the energy product.

Pressure sintering (hot isostatic pressing) techniques have also been used for densification of powder compacts. Close-to-theoretical values of density have been obtained using this process. Properties of magnets formed with very coarse powder (using this technique) were found to be quite comparable to what is available with present technology. With the use of finer-sized powder, magnets with outstanding properties are expected in the near future.

ACCESSION for	<input checked="" type="checkbox"/>
NTIS	<input type="checkbox"/>
DDC	<input type="checkbox"/>
UNANNOUNCED	<input type="checkbox"/>
JUSTIFIED	<input type="checkbox"/>
BY	
DISTRIBUTION/AVAILABILITY	RESTRICTED
	SPECIAL
A	

R-1177

MATERIALS RESEARCH FOR ADVANCED
INERTIAL INSTRUMENTATION

TASK 3: RARE EARTH MAGNETIC MATERIAL
TECHNOLOGY AS RELATED TO GYRO TORQUERS AND MOTORS

TECHNICAL REPORT
FOR THE PERIOD
30 SEPTEMBER 1977 - 30 JUNE 1978

July 1978

by

D. Das
E. Wettstein
K. Kumar

Prepared for the Office of Naval Research,
Department of the Navy, under contract
N00014-77-C-0388.

Approved for public release; distribution
unlimited.

Permission is granted the U.S. Government
to reproduce this paper in whole or in part.

APPROVED:


M. S. Sapuppo, Head
Component Development
Department

THE CHARLES STARK DRAPER LABORATORY, INC.
CAMBRIDGE, MASSACHUSETTS 02139

78 09 -07 001

ACKNOWLEDGEMENTS

We wish to express our appreciation to the National Magnet Laboratory, MIT, for their assistance by making their high field magnets available for our studies in this program. Our sincere thanks to C.R. Dauwalter for contributing the section on Magnet Stability Measurements.

This report was prepared by The Charles Stark Draper Laboratory, Inc. under Contract N00014-77-C0388 with the Office of Naval Research of the Department of the Navy, with Dr. F.S. Gardner of ONR, Boston, serving as Scientific Officer.

Publication of this report does not constitute approval by the U.S. Navy of the findings or conclusions contained herein. It is published for the exchange and stimulation of ideas.

TABLE OF CONTENTS

<u>Section</u>		<u>Page</u>
1	INTRODUCTION	1
2	OBJECTIVES	3
3	RATIONALE.	5
	3.1 Flux Stability at Constant Temperature	5
	3.2 Constant Flux at Varying Temperature Within Small Range	8
	3.3 Tailoring of Expansion Coefficient	10
4	PROGRAM.	11
	4.1 Overview.	11
	4.2 Plan.	13
5	DESCRIPTION OF THE SINTER MAGNET FACILITY.	15
6	HYSTERESIS MEASUREMENTS.	23
7	DEVELOPMENT OF A NOVEL MAGNET STABILITY MEASUREMENT DEVICE	25

TABLE OF CONTENTS (Continued)

<u>Section</u>		<u>Page</u>
8	EXPERIMENTAL ACTIVITIES	29
	8.1 General	29
	8.2 Powder Preparation	29
	8.3 Sintering.	32
	8.4 HIPping.	32
9	RESULTS AND DISCUSSION.	39
	9.1 Powder Preparation	39
	9.2 Sintering.	40
	9.3 HIPping.	46
10	CONCLUSIONS	53
	REFERENCES.	55

LIST OF FIGURES

<u>Figure</u>		<u>Page</u>
1	Saturation magnetic moment (σ_s) as a function of temperature of SmCo_5 and some HfCo_5 's.	9
2	Various steps in the sinter process.	12
3	Powder preparation machinery complex	16
4	Powder aligning and compaction assembly	18
5	Die and plungers	19
6	Soft iron flux focussing assembly around the die and plunger	19
7	A close-up of the die and plungers positioned in electromagnet to press Sm-Co disc	20
8	Sinter furnace facility.	21
9	A schematic diagram of the integrating fluxmeter.	24
10	The new configuration of magnetic circuit for stability measurement.	26
11	Particle size distribution in 34% Sm alloy powder used for sinter studies.	31
12	Particle size distribution in 42% alloy powder used for sinter studies	32

LIST OF FIGURES (Continued)

<u>Figure</u>	<u>Page</u>
13 Particle size distribution of -400 + 450 mesh fraction of 34% Sm alloy	33
14 Particle size distribution of -450 mesh powder of 34% Sm alloy.	34
15 Particle size distribution of -400 mesh 42% Sm alloy	35
16 A HIPped magnet inside stainless steel container and polished end of a few others	36
17 Micrograph of polished end of Sample H-7	37
18 Demagnetization curves of sintered Sample No. 1 of sinter run No. 7. (1) as sintered, (2) after anneal No. 1 and (3) after anneal No. 2.	43
19 H_{ci} , H_k versus Sm content of samples sintered at 1118°C.	44
20 H_{ci} versus sinter temperature and effect of optimum anneals for alloy composition 36% Sm.	45
21 Microstructure of Sample H-1 in as-HIPped condition. 200X magni- fication.	48
22 Microstructure of Sample H-5 in as-HIPped condition. 200X magni- fication.	49

LIST OF FIGURES (Continued)

<u>Figure</u>		<u>Page</u>
23	H_{ci} and H_k of HIPped Samples H-1 and H-5 in as-HIPped and annealed condition	51
24	Demagnetization curves of HIPped Sample H-5. Curve (4) as-HIPped, (5) after an anneal of 75 hours at 1000°C, and (6) further annealing at 900°C for 4 hours.	51

LIST OF TABLES

<u>Table</u>		<u>Page</u>
1	HIP sample designation and composition.	36
2	O ₂ content at various stages.	39
3	Sinter runs	41
4	Measured magnetic properties of sintered and heat treated samples	42
5	HIPped magnets.	47

SECTION 1
INTRODUCTION

The permanent magnet properties of Sm-Co magnets which make them extremely attractive for high performance applications are their very large intrinsic coercivity, H_{ci} , and maximum energy product $(BH)_{max}$. Because of the higher energy product, a smaller volume of the magnet will produce the necessary magnetic field strength for a given application. As such, it is an excellent characteristic of Sm-Co magnets. A great deal of improvement is not possible in this area. The large value of coercivity is a measure of the magnet's resistance to demagnetizing fields and therefore relates to its flux stability. Research is needed to further improve coercivity.

The thrust of the present program is to develop Sm-Co magnets for application in future generations of gyros, accelerometers and other components of inertial systems, where several orders of magnitude higher stability will be required than is available in present day commercial magnets⁽¹⁾. For our applications, the magnet should also have a constant residual induction over a small range of temperature and be compatible with beryllium in thermal expansion characteristics. The latter two requirements are not considered difficult to achieve as compared to the stability requirement of 8 parts per billion in ninety days. As already stated, the stable performance of a magnet is directly related to its resistance to demagnetization, or, its coercivity. To this we may add, that it should not only have a very high coercivity but that its hysteresis curve characteristics must be as nearly a rectangular loop as possible.

Faint, illegible text, possibly bleed-through from the reverse side of the page.

blank
2

SECTION 2
OBJECTIVES

The objectives of the present program are to develop improved sintering procedures to produce inertial grade Sm-Co magnets with improvements in the following areas:

- (1) Long term flux stability at constant temperature (140°F)
 - Desired 0.008 ppm/90-day
 - Present capability 3 to 12 ppm/day

- (2) Thermal stability of residual induction -
 - Desired 0.1 ppm/°F
 - Present Capability 300 ppm/°F

- (3) Tailoring of thermal expansion coefficient -
 - Desired, same as beryllium
 - Isotropic 2.8 $\mu\text{in/in}^\circ\text{F}$
 - Oriented: 5.6 $\mu\text{in/in}^\circ\text{F}$
 - (a) along magnetization direction 2.8 $\mu\text{in/in}^\circ\text{F}$
 - (b) vertical to magnetization direction 7.2 $\mu\text{in/in}^\circ\text{F}$

SECTION 3

RATIONALE

3.1 Flux Stability at Constant Temperature

Of the three objectives listed in the previous section, the first one is the most important and required a careful analysis of theory and experimental data involved to formulate a plan of attack⁽²⁾. Based on the above analysis we arrived at the conclusion that we would have to improve both the intrinsic coercivity and the general characteristics of the second quadrant of the (B-H) curve. In order to obtain the above magnetic behaviors the structural requirements from the materials point of view would be to produce a highly densified (93 percent of theoretical or better) sintered body comprised of very fine crystallites with the fewest number of defects possible.

The anisotropy magnetic field of the compound SmCo_5 is about 350 kOe. The hexagonal SmCo_5 crystal reaches its saturation magnetization of about 10 kG when a magnetic field of no higher intensity than 10 kOe is applied along its easy magnetizing direction, which happens to be its C-axis. However, in order to reach saturation, the field applied parallel to the basal plane of the crystal has to be 350 kOe. The physical implication of the above facts is that a single domain SmCo_5 particle (smaller than $1.6 \mu\text{m}$ in any direction⁽³⁾) containing zero defects would require a reverse magnetic field of 350 kOe to completely reverse its magnetization. In other words, the intrinsic coercivity of this particle is 350 kOe. A SmCo_5 magnet body composed of densely

packed particles of the above description would have a residual induction (B_r) of 10 kG, H_{ci} of 350 kOe, a $(BH)_{max}$ of 25 mGOe and an absolutely perfect rectangular hysteresis loop of gigantic proportions. The above structural features appear unattainable under terrestrial conditions. The main cause of the defects is the ever-present oxygen in the magnets. One of the primary objectives of the program is to reduce the oxygen content of the magnet.

Clearly, the demagnetization process of sintered Sm-Co magnets is not a result of the vector rotation of magnetization. If it were a rotational process, the intrinsic coercivity would be 350 kOe instead of only 15 to 30 kOe which is generally found in commercial magnets. The mechanism of demagnetization is actually a process of nucleation and growth of reverse domains under the influence of a reverse magnetic field at defect sites in a crystallite. Once a nucleated domain reaches a critical size, it easily sweeps across the entire grain with little or no increase in the intensity of the applied reverse field. The magnitude of the required reverse field for the reversal of magnetization can vary from very small (self-demagnetizing field) to very high field (many decades of kOe) intensity. A magnet body comprised of millions of crystallites would therefore demagnetize over a wide range of applied field. The larger the number of defects in a crystal, the more likely it is to reverse at a lower field. A magnet that has a lower coercivity than another must therefore have more defects per crystal. A magnet with larger grain size is found to have more defects per crystal and therefore should and does have lower coercivity.

Coercivity, as has already been shown^(4,5), is related to the long-term flux stability of a magnet. And from the reasons we have given above, coercivity is seen to be directly related to the number of defects per crystal. With a given number of defects per unit volume of a magnet it will definitely be profitable to have the grain size as small as possible to obtain fewer defects per crystal. Thus, we have defined one of the two structural requirements for a more stable magnet. The grain size in the magnet must be as small as possible.

The discussion so far has been the reversal of magnetization initiated by defects present in the magnets. There are a number of kinds of such defects, but the ones that are known to be the most significant contributors are due to the presence of foreign atoms in the alloy. Two important sources of the contamination by foreign atoms are the crucibles used for melting the alloys and the oxygen in the air which invariably comes in contact with the alloy and its powder during processing. Since the alloy must be prepared by melting Sm and Co together, there is bound to be some contamination from the crucible walls. It can be minimized by proper melting procedures. The amount of oxygen pickup can also be controlled to a certain extent, but it is practically impossible to completely eliminate it. Commercial sintered magnets contain between one and two weight-percent oxygen.

Research recently conducted at The Charles Stark Draper Laboratory, Inc. (CSDL), has provided strong evidence of the damaging influence of oxygen on the coercivity and the coercivity-retaining ability of Sm-Co magnets. The oxygen content in the CSDL arc-plasma-sprayed magnets is less by an order of magnitude than in commercial magnets. Sprayed magnets also have almost twice the coercivity⁽⁶⁾. In addition, these magnets are greatly resistant to degradation in H_{ci} from the same thermal processing that is known to be severely detrimental to commercial sintered magnets. This increased coercivity-retaining ability is believed to be directly related to the lesser amount of oxygen in the material⁽⁷⁾. Dissolution and reprecipitation processes involving oxygen are known to result in localized composition inhomogeneities which are composed of low anisotropy (and therefore low coercivity) material^(7,8).

An insight into the effect of oxygen on coercivity of Sm-Co magnets is provided by the excellent study by Bartlett and Jorgensen⁽⁸⁾ on microstructural changes in $SmCo_5$ crystal due to the presence of oxygen accompanying the processing of Sm-Co magnets. The solubility of oxygen in $SmCo_5$ is 0.35 to 0.4 weight percent at 1100°C (sintering

temperature) in excess of the solubility at 800°C. Therefore on cooling from the sintering temperature submicron size particles of Sm_2O_3 precipitate within the SmCo_5 grain accompanied by a depletion of Sm in the surrounding regions. The depleted regions form $\text{Sm}_2\text{Co}_{17}$ particles which are of much lower anisotropy than SmCo_5 . In the light of their investigations, the variation in coercivity observed by many workers (9,10,11,12,13,14) can be explained as directly related to the dissolution and precipitation phenomenon of oxygen in SmCo_5 . So here is our second requirement, which is a reduction of defects in the SmCo_5 crystallites by reducing the amount of oxygen in them.

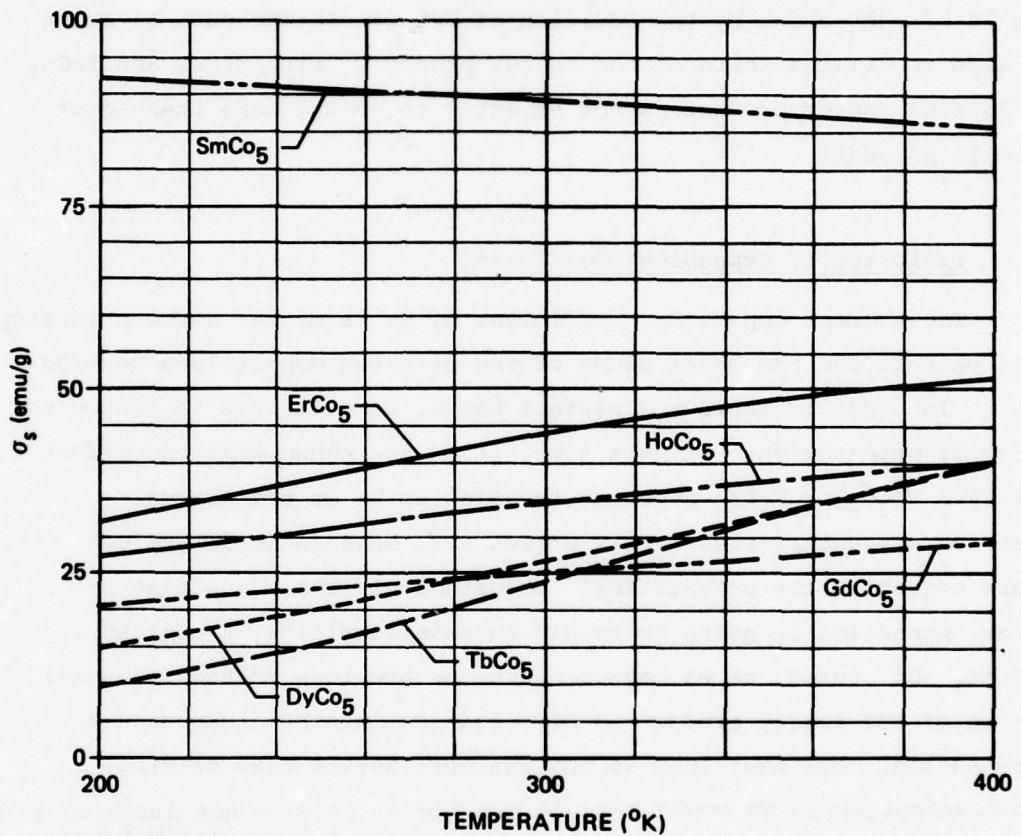
A third requirement for stable performance at constant temperature is a sufficiently densified body whose internal porosity is isolated from the surface. This is of no great concern since practically all sintered Sm-Co magnets meet this requirement by densifying the body to 93 percent or higher. Normal sintering at around 1100°C produces that kind of density.

3.2 Constant Flux at Varying Temperatures Within Small Range

Loss of residual induction of a magnet on taking it up to an elevated temperature below its Curie temperature is composed of two parts: irreversible and reversible. On cooling down to room temperature, the reversible loss is restored, but the irreversible loss can be regained only by remagnetization, provided there has been no structural change caused by the thermal cycling. Assuming that to be the case, the magnet, after the first thermal treatment, will retrace the same induction versus temperature curve on repeated thermal cycling between room temperature and the particular higher temperature.

SmCo_5 shows a continuous decrease of flux at a rate of approximately 400 ppm/°C within a temperature range of R.T. to 250°C. All light rare earths show similar behavior as Sm. However, the heavier rare earths (HRE) such as Er, Ho, Dy, Gd and Tb have an initial increase before they start to decrease towards zero at Curie temperature (15,16). From the above two references we have replotted the data on saturation

magnetization of the heavy rare earth - Co₅ compounds along with those of SmCo₅ for the temperature range of 200°K to 400°K in Fig. 1. This includes the temperature of interest for us. Because of the opposite signs of temperature coefficients between that of SmCo₅ and the HRE Co₅ one would expect that a rare-earth composition balanced between Sm and any of the HRE's would result in a zero temperature coefficient.



12/77 CD13030

Figure 1. Saturation magnetic moment (σ_s) as a function of temperature of SmCo₅ and some HRECo₅'s.

Studies done elsewhere (17,18) have shown such results using the two HRE elements Gd and Ho in conjunction with Sm. It takes approximately 20 percent Ho and 40 percent Gd to achieve near-zero temperature coefficient. The slopes of TbCo₅ and ErCo₅ are much higher than either HoCo₅ and GdCo₅. It will therefore require a much smaller amount of ErCo₅ or TbCo₅ to achieve the zero temperature coefficient. The result, of course, will be that we will not have to sacrifice as much of the energy product. This is important in view of the fact that almost 50 percent of the energy product is lost when perfect temperature compensation is brought about by the addition of GdCo₅. In the case of HoCo₅ the loss is still a third of the energy product. With ErCo₅ and TbCo₅ the loss of energy product is not expected to be any more than about 10 to 15 percent.

3.3 Tailoring of Expansion Coefficient

The thermal expansion coefficient of Be is midway between isotropic SmCo₅ magnets and the basal plane of the oriented magnet [see Section 2(3)]. In order to achieve a perfect match, we will have to reduce the degree of orientation. At this time, it is not known what the effect of either TbCo₅ or ErCo₅ addition is going to be on the thermal expansion characteristics. This effect will have to be determined before adjusting the orientation. Unfortunately the adjustment of thermal expansion is going to result in some sacrifice in the energy product. Of course, as we have seen in the previous section, a small portion of the energy product is also lost in internal temperature compensation. But that loss is not any more severe than external compensation, which we would have to provide if it were not internally compensated. Internal compensation is less complicated, requires less material, and should be more stable, not depending on the physical location of a compensator relative to the magnet.

SECTION 4 PROGRAM

4.1 Overview

The program is aimed at producing highly stable and temperature compensated sintered Sm-Co magnets from powders (prepared from alloys of Sm and Co). In order to obtain the desired properties the densified magnets should be composed of fine grains with minimal defects by greatly reducing the oxygen content in the final product.

Oxygen contamination occurs during powder preparation and subsequent processing. All powder preparation, alignment, compaction and sintering operations are being conducted in extremely clean environments. The thermal processes will be developed which would greatly minimize the residual stresses. Slow cooling cycles will be employed following the high temperature treatments. If that procedure results in loss of properties then stress relieving treatment after fast-cooling rates will be considered as an alternative.

The sinter process program plan is shown in Fig. 2, with various action items in designated boxes. Shaded area in various boxes indicate whether the action has commenced and the amount of shaded area denotes the level of completion of the item. Although a large number of the boxes are completely shaded and would tend to indicate that the program is nearly completed, the fact is that the program has a good start and is beginning to roll along. Detailed investigations of sintering cycles, optimizing heat treatments, temperature compensation studies, stability evaluation, etc. are yet to be performed.

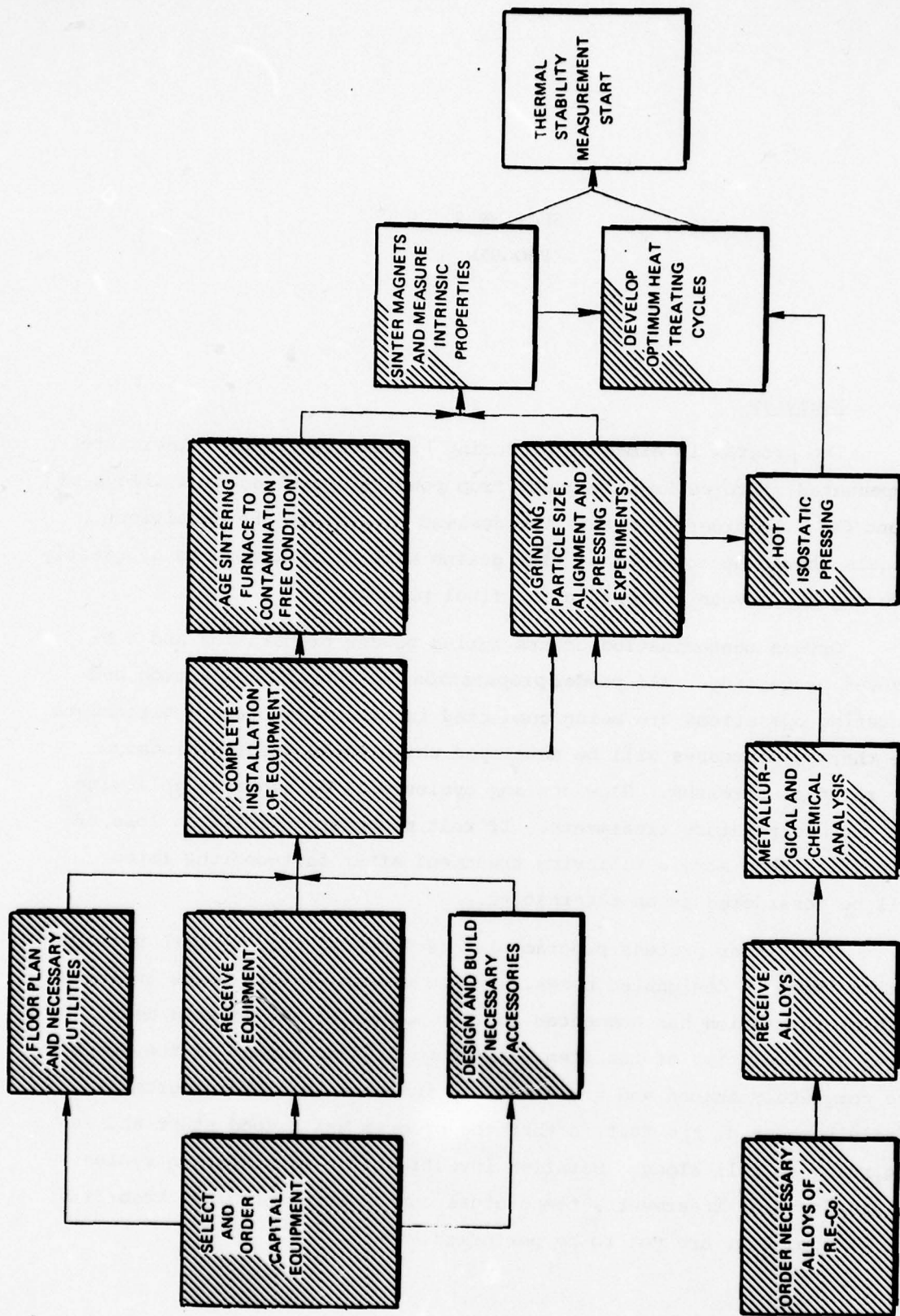


Figure 2. Various steps in the sinter process.

1/77 10702 REV C 8/78

4.2 Plan

The specific tasks are as follows:

- (1) Optimization of powder preparation.
- (2) Optimization of composition by blending two alloys.
- (3) Optimization of alignment, pressing, sintering, and heat treatment for maximum intrinsic properties.
- (4) Pressure sintering (hot isostatic pressing) and optimizing heat treatment for even better properties.
- (5) Blending SmCo_5 and HfE- Co_5 for temperature compensation.
- (6) Controlled variation of alignment for thermal expansion matching.
- (7) Development of the understanding of the above items in their physical phenomena.
- (8) Stability measurements and relating these determinations to physical and magnetic properties.

SECTION 5
DESCRIPTION OF THE SINTER MAGNET FACILITY

Since all the alloys required for this program are being purchased from commercial sources, no alloy melting equipment was required. It is also possible to purchase alloy powders from vendors. However, our initial experience with purchased powders for use in the Arc-Plasma-Sprayed Magnet Program revealed that the preparation process used by vendors lacked adequate control in two areas of great importance:

- (1) Minimization of oxidation during preparation, and
- (2) Particle size and size distribution.

As a result of the above experience, we decided that we would have to prepare our own powder for our experiments. However, we would continue to purchase the alloys, which were to be prepared to meet our specifications. In preparation for the ONR sponsored effort, CSDL provided a Sm-Co magnet research laboratory with the following essential functions:

- (1) Powder preparation with controls on -
 - a. particle size and size distribution
 - b. minimal oxidation
 - c. blending of alloy powders to obtain desired composition
- (2) Compaction of powder in an aligning field.
- (3) Sintering and thermal optimization treatments in an ultraclean environment.

Fig. 3 shows the powder preparation facilities for the Sm-Co magnet program, consisting of a Jaw crusher, a double disc pulverizer, an attritor ball mill and a blending machine with two stainless steel blender shells. In addition, we have also installed a Ro-tap sieving machine mounted inside a soundproof box.

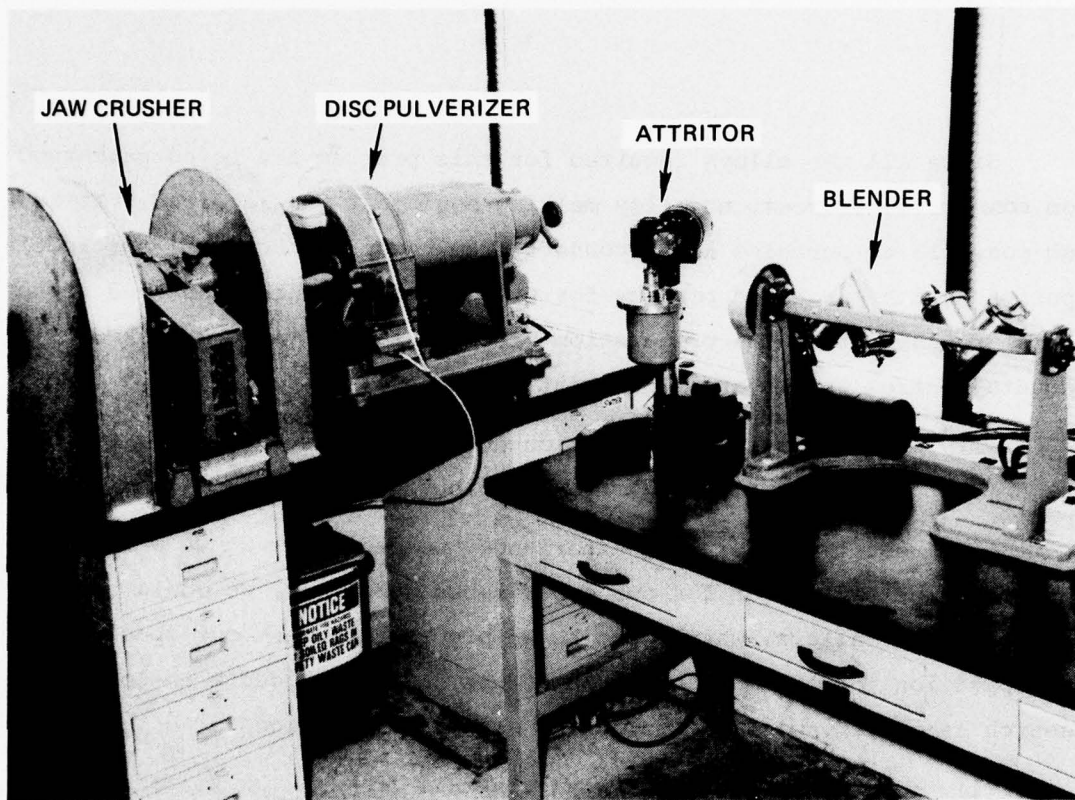


Figure 3. Powder preparation machinery complex.

The powder compaction system is shown in Fig. 4. A 30-ton motor-driven press is shown located at the center, in pressing position. An electromagnet capable of producing 20 kOe aligning field for a 1/2 inch diameter disc sample is mounted on the lower platten. The magnet was designed and built by The Charles Stark Draper Laboratory (CSDL). To the right of the press is a 10 kw dc power supply also designed and built at CSDL, for the electromagnet. On the left is a 1 kw pulsed power supply which can energize a pulsed coil within the electromagnet cavity with half-millisecond 20 kOe pulses once every 30 seconds. This level of pulsed field may or may not give a much better aligned magnet over what is done with the 20 kOe dc magnet. There are plans right now to modify the present pulser with an additional bank of capacitors to provide a pulse energy of 10 kw which will give us 50 kG pulses of 2 millisecond duration once every minute. This will be a sufficient boost in magnet alignment to increase the maximum energy product from about 16 mGOe to 20 mGOe.

A higher energy product magnet will possibly possess higher stability because of better alignment and more uniform density and thus better match the thermal expansion coefficient of adjacent grains. The additional energy product will, of course, be a welcome bonus.

The die and plunger, designed by CSDL, are shown in Fig. 5. The plungers are hardened tool steel which can easily withstand pressures of 100 Klb/in². The outer shell of the die is constructed of three layers, the top and bottom being hardened tool steel and magnetic. The middle is nonmagnetic. A highly polished tungsten carbide sleeve is press-fitted into the composite die and provides the smooth wall for low friction during compaction. The magnetic flux is focussed axially through the die to a value of 20 kOe. The focussing assembly is shown in Fig. 6. Fig 7 is a closeup of the electromagnet on the press platten with the die and plungers in the focussing assembly in position inside the electromagnet.

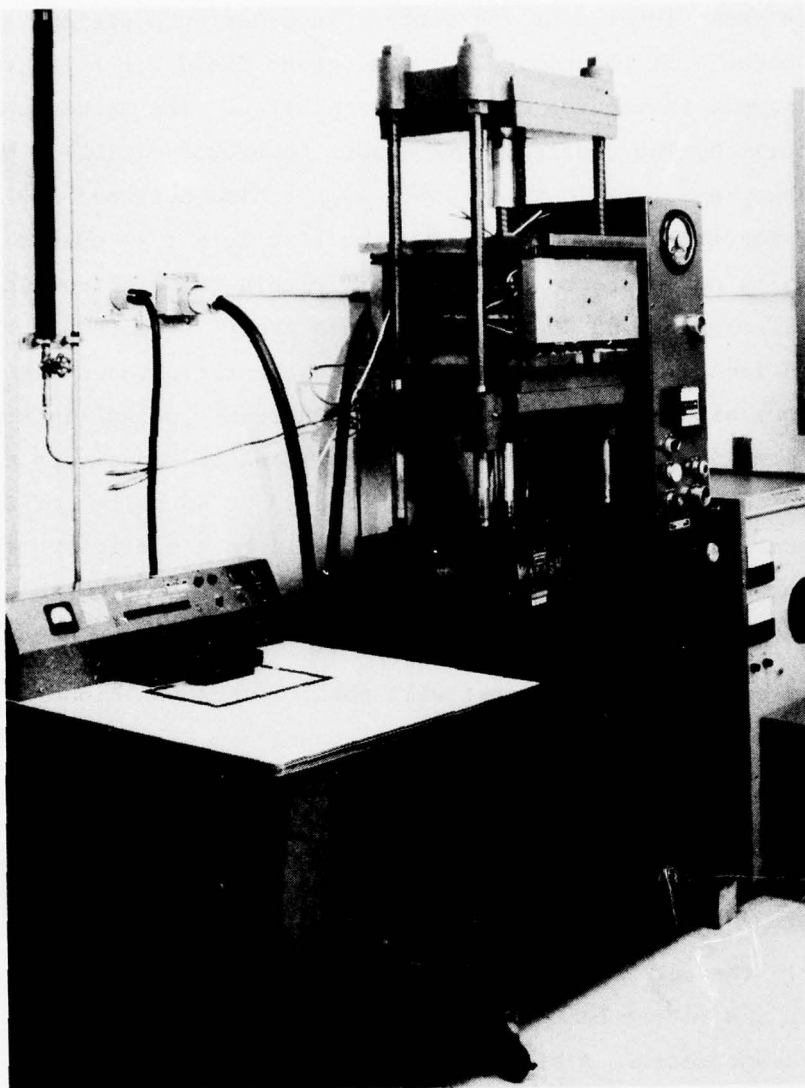


Figure 4. Powder aligning and compaction assembly.

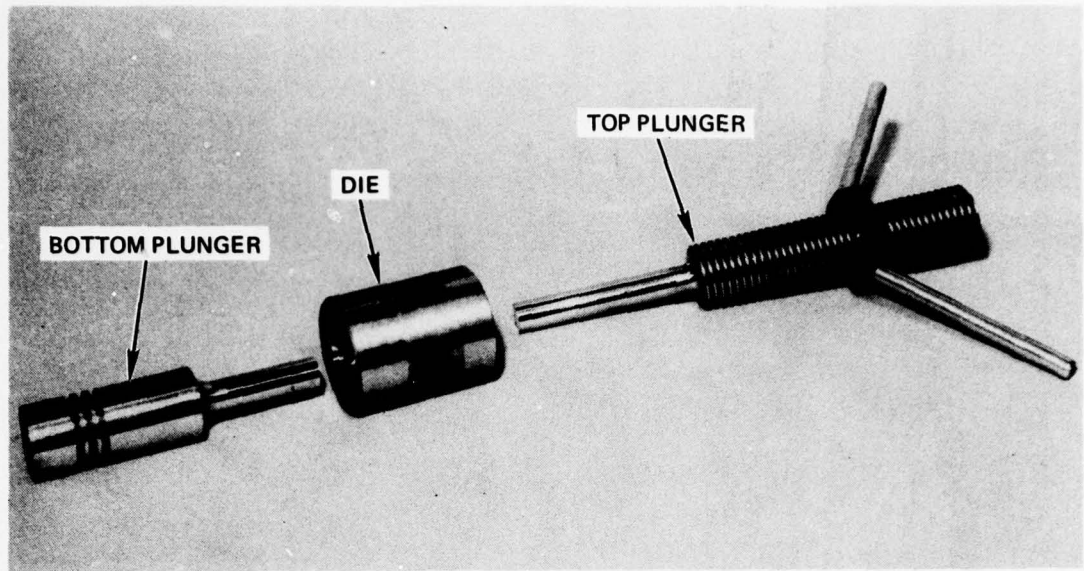


Figure 5. Die and plungers.

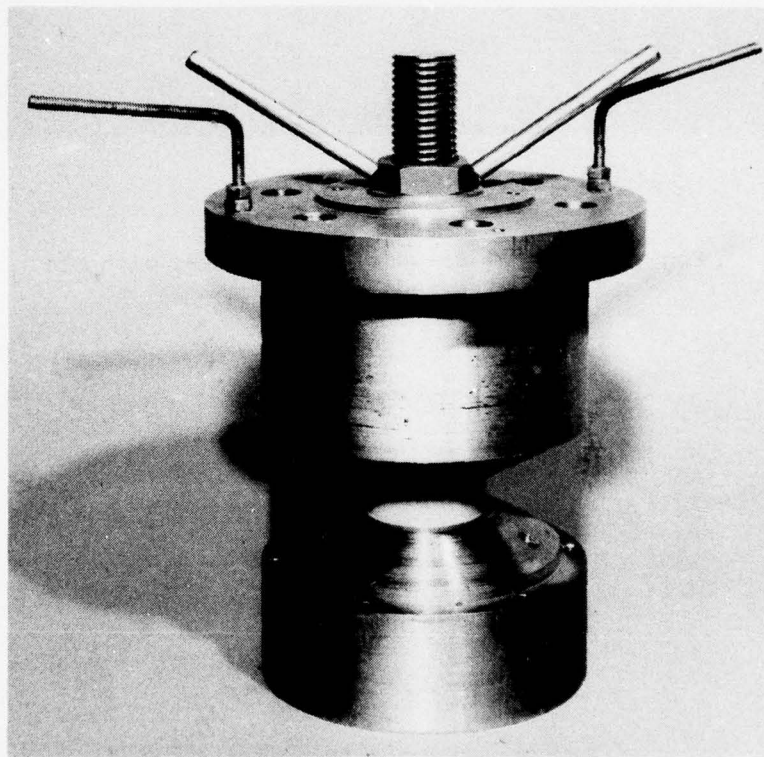


Figure 6. Soft iron flux focussing assembly around the die and plunger.

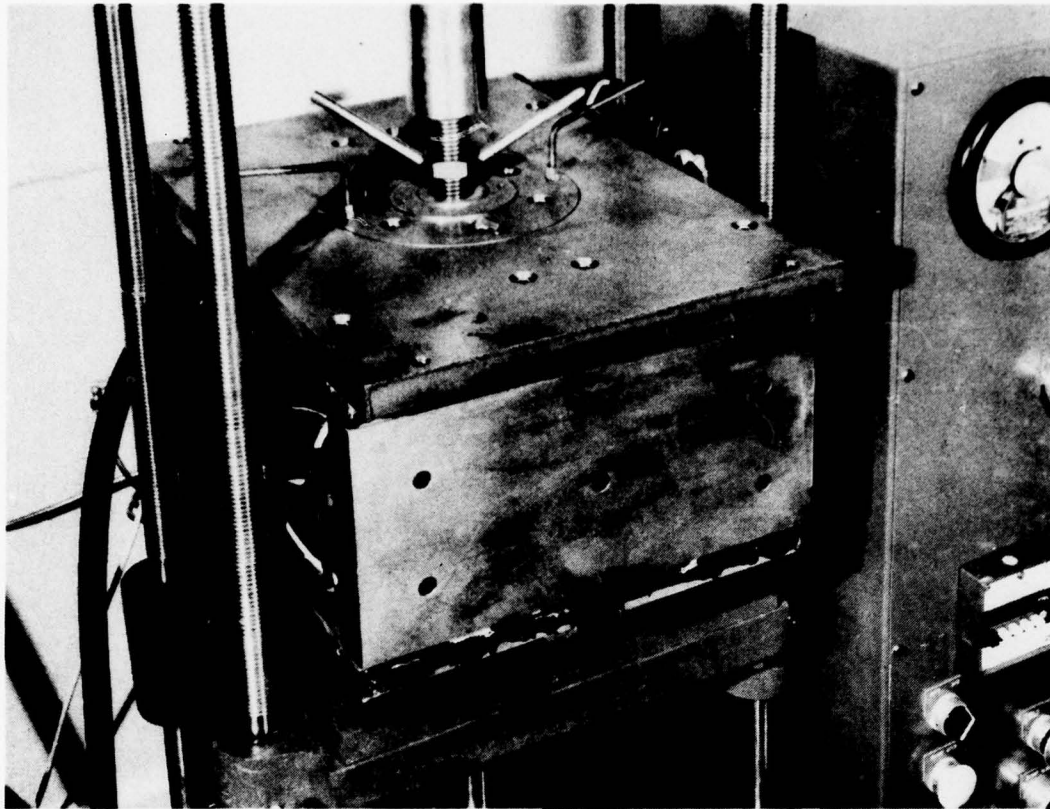


Figure 7. A close-up of the die and plungers positioned in electromagnet to press Sm-Co disc.

The sinter furnace assembly is shown in Fig. 8. The furnace is on the table top with its 1/2 inch thick wall Inconel muffle. Behind this furnace is a small tube furnace for purification of helium, which enters the sinter muffle at the end on the right-hand side. The magnet samples are placed in or taken out through the flanged end on the left-hand side. A 1-1/2 inch stainless tube connects the furnace to the pumping system below consisting of a mechanical pump, a diffusion pump and a liquid nitrogen trap. The valving arrangement in the system permits isolation of the furnace from either the pump or the gas flow system.

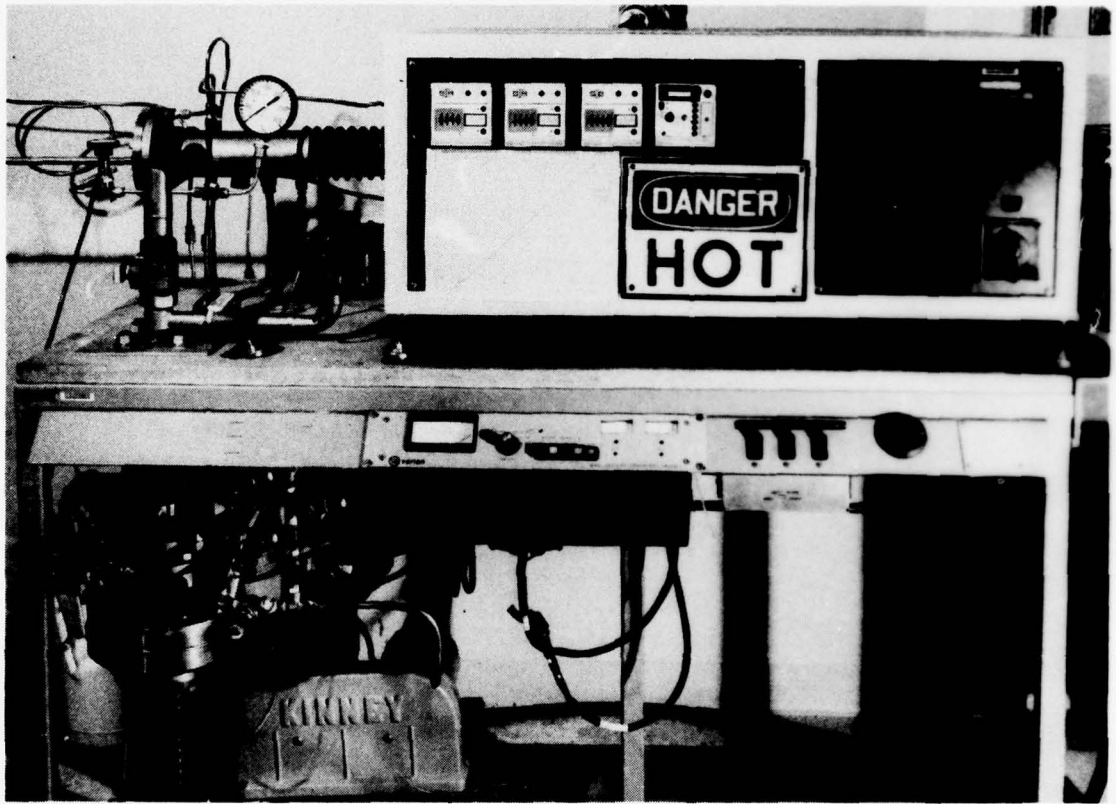


Figure 8. Sinter furnace facility.

Because of the heavy wall thickness of the Inconel muffle, it required several months of outgassing before the first sintering run was made. The system is now highly clean and we can reach 10^{-6} torr range vacuum with the furnace running at 1100°C . However, we do expect to run most of our sintering experiments in helium atmosphere after a bakeout in vacuum at 400°C prior to introduction of gas. The experiments until now have been at approximately one atmosphere pressure (flowing gas). However, we expect to run some experiments at considerably higher pressure. Calculations show that the muffle is capable of withstanding 2000 lb/in^2 of gas pressure at 1000°C , which is more than what we expect to use.

SECTION 6
HYSTERESIS MEASUREMENTS

The magnets produced at CSDL are now being measured at the National Magnet Laboratory in fields up to 150 kOe. An X-Y recorder traces $4\pi M$ versus H. $4\pi M$ is obtained from an integrating fluxmeter with two coils. One of the coils measures the magnet flux and the other the air flux. In a bucking position, these supply the $(B - H = 4\pi M)$ signal. The H signal is obtained directly from the control panel of the Bitter solenoid. A schematic diagram of the integrating fluxmeter is shown in Fig. 9.

The integrator has to be of high stability in order to prevent a drift in the output voltage during measurements. Our present instrumentation shows a drift of less than one percent in five minutes. This low level of drift is obtained by using a high quality integrating capacitor, and coils with a large number of turns (5,000).

For calibration, a nickel sample of identical size as the magnet is used. Small deviations in size cause signal changes proportional to the volume change. The selfdemagnetizing field of the magnet causes a shearing of the hysteresis curve. The curves are corrected by tracing the $4\pi M$ axis through known points relative to the nickel curve.

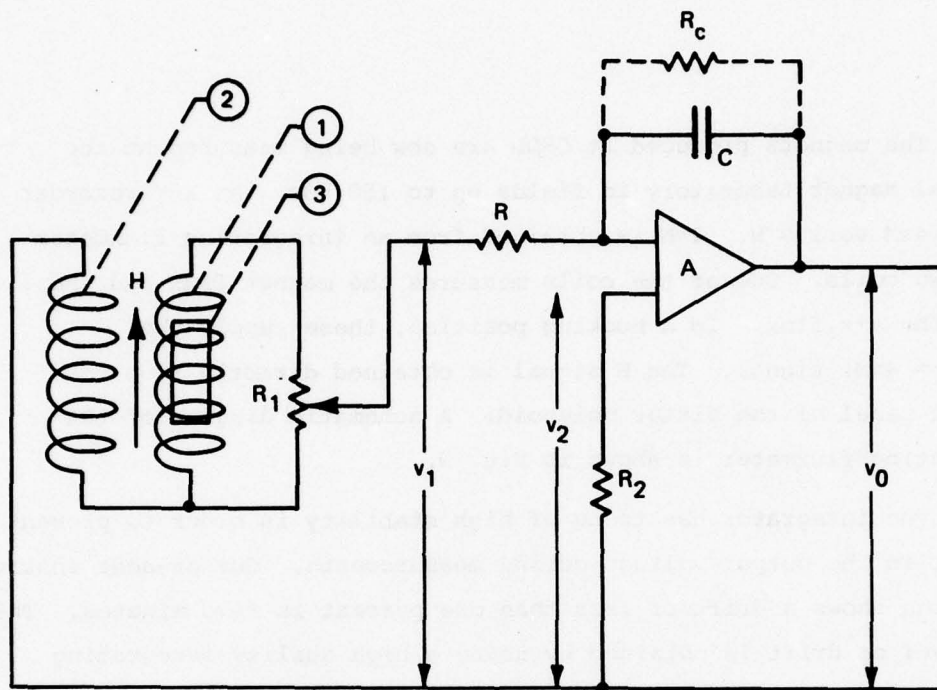


Figure 9. A schematic diagram of the integrating fluxmeter.

SECTION 7
DEVELOPMENT OF A NOVEL MAGNET STABILITY
MEASUREMENT DEVICE

When a multipole magnet structure is rotated in an electric generator circuit at a constant speed (an easily controllable experimental parameter) a voltage is produced in the generator coil which is proportional to the magnetic flux density and the speed of the rotor. With the speed remaining constant, any change in the output voltage is due only to a change in the magnetic flux density. The output voltage which can be measured with great precision, gives us a direct and quantitative measurement of the stability of the magnets.

Stability evaluations of SmCo_5 magnets have, to date, been performed using a multipole magnetic structure originally designed for a permanent magnet torque generator utilizing Alnico IX. This was expedient because the required hardware and test fixtures were available and the evaluations could be started quickly and undertaken inexpensively. The arrangement, however, presents several problems:

- (1) Twelve magnets, machined to relatively close tolerances, are required for each evaluation. Each of the magnets should, preferably, be cut from the same sample, which is sometimes impractical and always expensive.
- (2) The magnets must be individually magnetized prior to being cemented into the structure; this submits them to a thermal prestabilization cycle which may be undesirable when the objective is to examine the natural stability of the magnets. Also, considerable time necessarily elapses between magnetization and the beginning of measurement.

A new magnetic circuit configuration is being investigated, which promises significant advantages compared to the former one. The new configuration, shown in Fig. 10, has the following features:

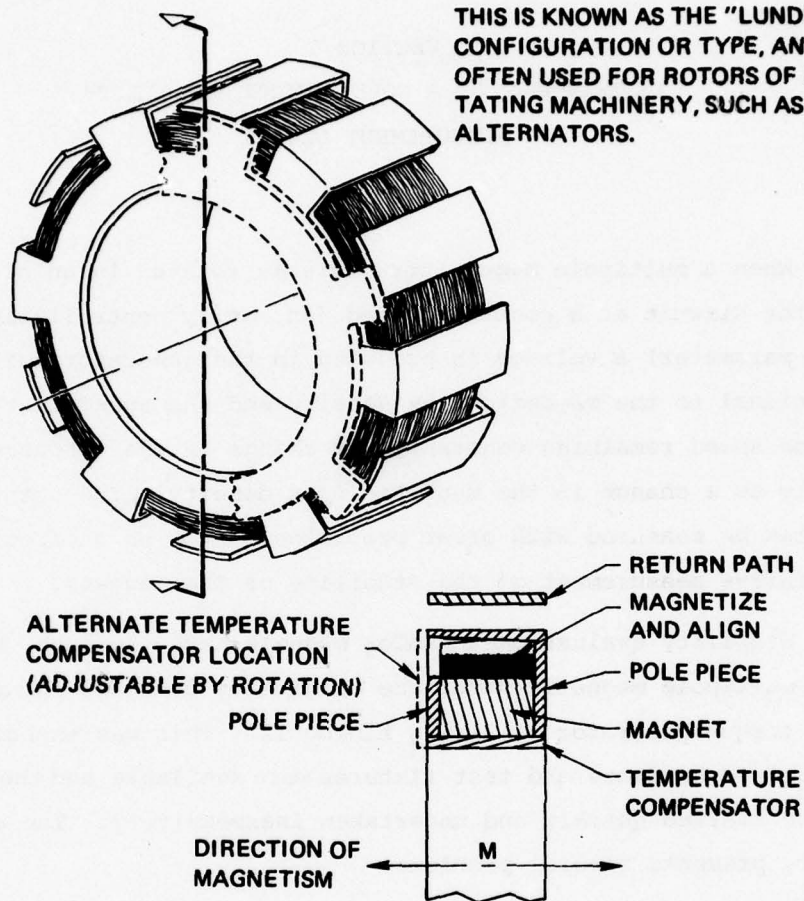


Figure 10. The new configuration of magnetic circuit for stability measurements.

- (1) A single, cylindrical, magnet is required for each test. This shape is compatible with both sintered and arc-plasma-sprayed fabrication processes and the only critical dimension is parallelism of the end faces.

- (2) The magnet can be cemented into the magnetic circuit (or, alternatively, could be mechanically clamped) prior to magnetization because the magnetization is along the cylinder axis. Thus, no (possibly unwanted) thermal prestabilization need be applied. Additionally, the magnet can be assembled and magnetized and temperature compensation adjusted prior to the final magnetization preceding the test. Consequently, stability testing can commence almost immediately following final magnetization. Since magnets decay logarithmically with time following magnetization, the rate of change of remnance is most rapid immediately following magnetization and becomes progressively slower with the passage of time. Clearly, with a fixed measurement error, the most accurate results can be obtained, or results of a given accuracy can be obtained, in a shorter time if measurements are started as soon as possible following magnetization.
- (3) The operating flux density can be easily altered by changing the sample diameter. This facilitates evaluation of the effect on stability of operating point. Such evaluation can be conducted on a single sample by progressively reducing its diameter thus reducing or eliminating any effects of sample-to-sample variations on the results.

SECTION 8 EXPERIMENTAL ACTIVITIES

8.1 General

A very carefully planned experimental effort has gone into the magnet program so far and includes the following activities:

(a) Designing and building of magnetic aligning and pressing fixtures, sinter furnace components, magnetic hysteresis measurement instrumentation and modification of stability measurement devices; (b) installation and testing of various components of the sinter facility; (c) a three-month long outgassing of the sinter furnace; (d) powder preparation techniques and analytical procedures: (e) a good start on sintering and (f) started using pressure sintering (hot isostatic pressing) for densified Sm-Co powder magnets.

Items (a), (b) and (c) have already been adequately described in Section 5. Therefore, here we will dwell on the three areas of experimental activities, viz, powder preparation, sintering and HIPping.

8.2 Powder Preparation

Powder preparation is considered to be one of the most important steps in the overall process of producing high stability Sm-Co magnets. On the one hand, in order to produce high coercivity, which determines stability, the powder particle size must be very small. At the same time, we must also minimize the oxygen content of the final sintered magnet. Unless all the steps involved in the fabrication can be carried out without exposure to air until after the final densification

the two requirements are difficult to meet simultaneously. Therefore, a compromise is sought, coupled with extreme care to prevent oxidation of the powder. We had developed some expertise in the preparation of coarse Sm-Co powder for our arc-plasma-sprayed magnets. We had begun to produce powders with substantially less oxygen than in the purchased powder. As a result, we now have a powder preparation technique which is quite satisfactory both from the size and oxygen contamination points of view, which is as follows:

- (1) As received alloy is reduced to -1/4 inch size in a jaw crusher. The operation is carried out in air.
- (2) The -1/4 inch size alloy is then pulverized in the double disc pulverizer which is flooded with argon. The gas enters the enclosed region through the feed hopper between the discs, and the tightly sealed box to receive the pulverized powder. The adjustable gap between the discs controlling the upper limit on the powder was set at 0.020 inch (500 μ m) opening. The output of the pulverizer is sieved through a 325 mesh screen and the minus portion (less than ten percent) is rejected.
- (3) The +325 mesh powder is ground for 25 minutes in the attritor using Toluene as a fluid vehicle. The excess Toluene is poured out and the powder dried on a watch glass in a ventillated hood.
- (4) The powder produced by the attritor mill is characterized in the following manner:

Particle size distribution using a π MC particle size analyzer (see Figs. 11 and 12).

X-ray fluorescence for bulk chemical composition.

Oxygen determination by vacuum fusion.

(5) Two alloys of compositions 34 percent Sm-balance Co and 42 percent Sm-balance Co (to correspond to the compounds SmCo_5 and Sm_2Co_7 respectively) were used. Powders of various compositions within the range of above compositions were produced by blending calculated amounts of each powder in the blending machine.

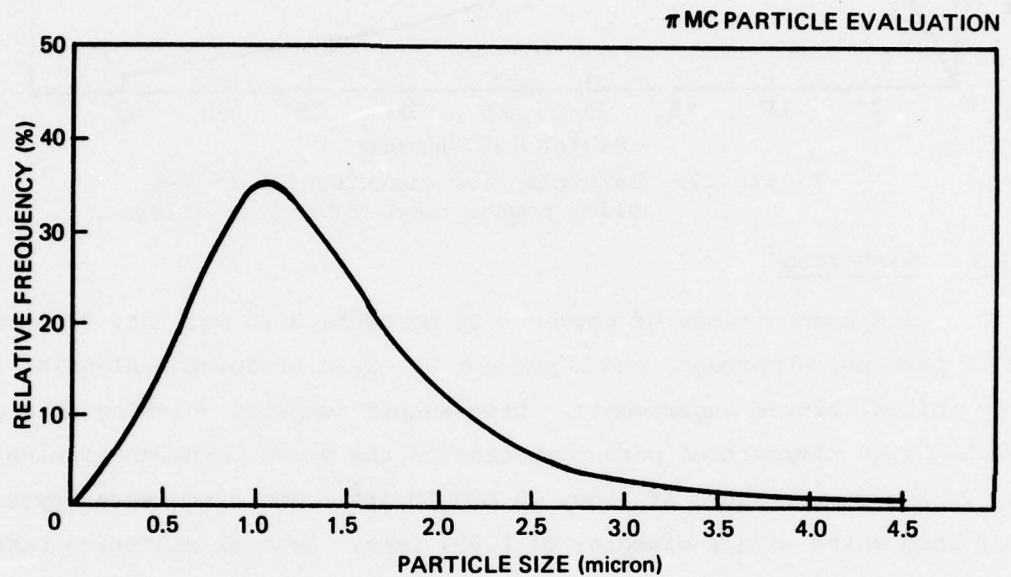


Figure 11. Particle size distribution in 34% Sm alloy powder used for sinter studies.

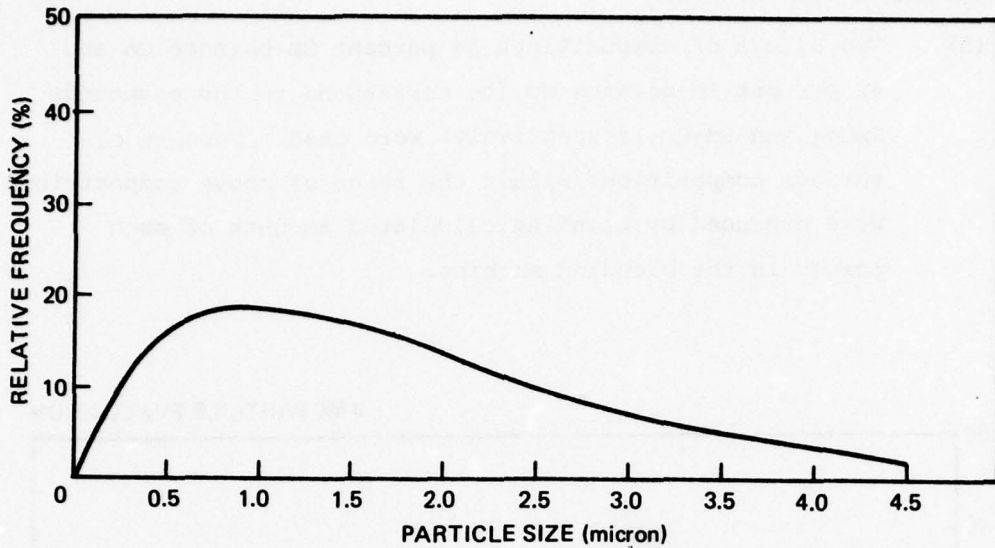


Figure 12. Particle size distribution in 42% alloy powder used for sinter studies.

8.3 Sintering

Six compositions of powder - 36 percent, 36.5 percent, 37 percent, 37.5 percent, 38 percent, and 39 percent Sm - were produced by blending for the initial sinter experiments. Disc-shaped compacts weighing four grams each of each composition were compacted in the press using an aligning field of 20 kOe at a pressure of about 75,000 lb/in². The discs were approximately 1/8 inch thick with a diameter of 0.557 inch. Several sintering runs were made varying the sinter temperature between 1100°C and 1124°C for one and one-half hours' holding at the preselected sintering temperature and cooling down the furnace overnight. In one case the sintering was done in vacuum.

8.4 HIPping

The program as originally proposed did not include any HIPping experiments. However, subsequent to the generation of this proposal and prior to the initiation of this program we conducted HIPping experiments on other Sm-Co magnets with very favorable results such as close to 100 percent density and no grain growth. These results dictated the inclusion of HIPping as a method for the present studies related to high stability magnets. Our initial experiments of hot isostatic pressing of Sm-Co magnets were carried out at 900°C under a pressure of 15,000 lb/in². We chose to stay with the above experimental parameters.

Four compositions - 35.5 percent, 36.5 percent, 37.5 percent and 38.5 percent Sm - were chosen for the initial experiments. These were obtained by blending the 34 percent Sm and 42 percent Sm alloy powders. Since no grain growth was expected, we decided to use fairly coarse powders. We ground the pulverized Sm-Co alloy powders for only about three minutes in the attritor ball mill (compared to 25 minute grinding for sintering). The powders were sieved through 400 mesh screen. The -400 mesh portion of the 34 percent alloy was then further sieved through 450 mesh screen giving two fractions; a -400+450 mesh powder and a -450 mesh powder. The additive alloy (42 percent Sm) was used only in the -400 mesh size. The particle size distributions of these three fractions - two of 34 percent and one of 42 percent - are shown in Figs. 13, 14 and 15. In Table 1, the sample designations, the mixing components and blended sample compositions are shown.

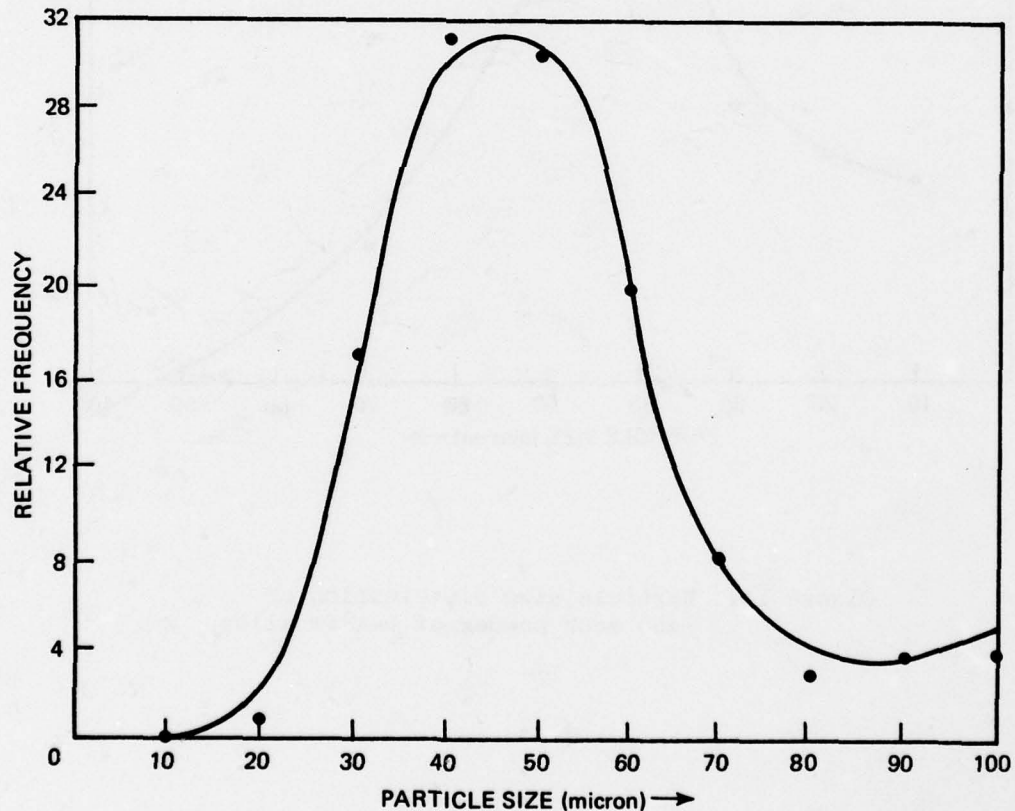


Figure 13. Particle size distribution of -400+450 mesh fraction of 34% Sm alloy.

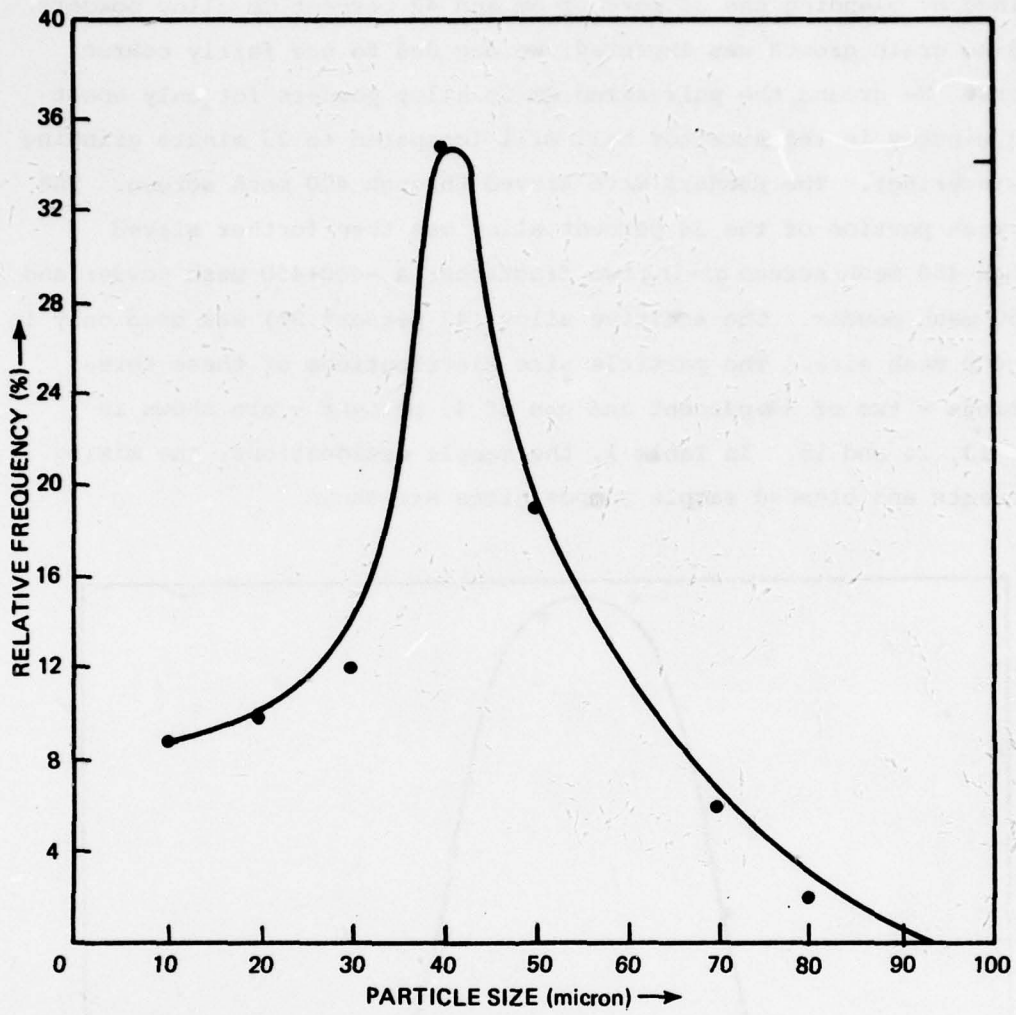


Figure 14. Particle size distribution of
-450 mesh powder of 34% Sm alloy.

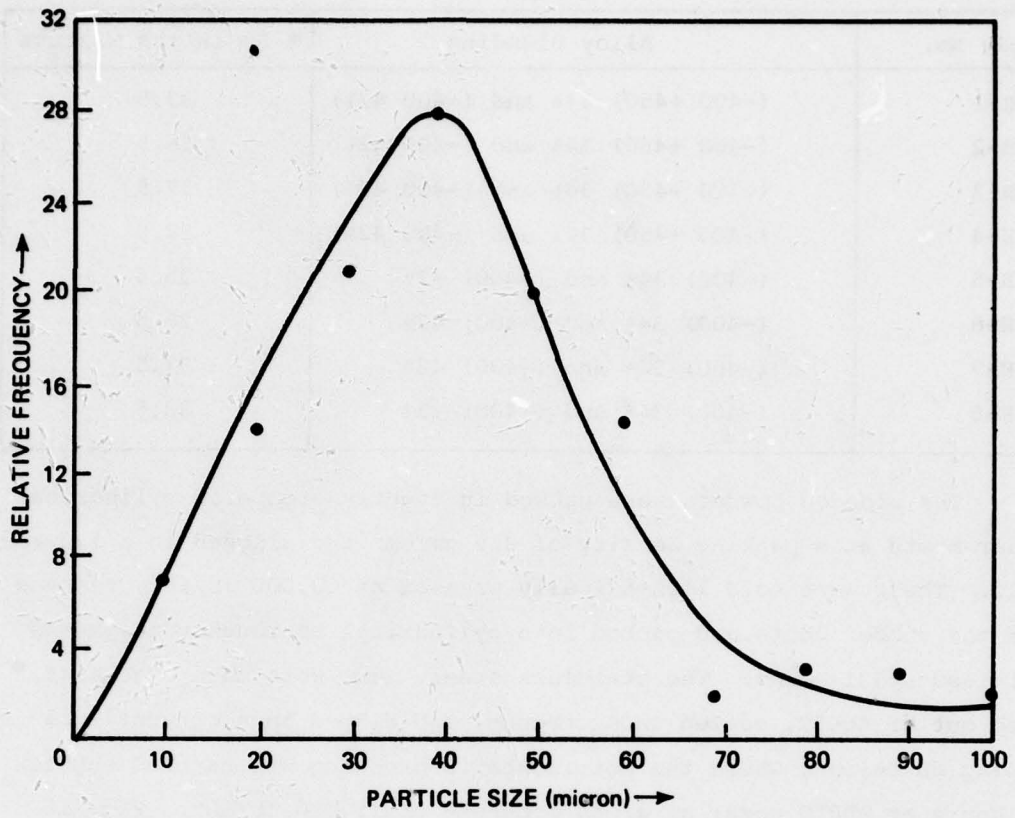


Figure 15. Particle size distribution of
-400 mesh 42% Sm alloy.

Table 1. HIP sample designation and composition.

Sample No.	Alloy Blending	% Sm in the Mixture
H-1	(-400 +450) 34% and (-400 42%)	35.5
H-2	(-400 +450) 34% and (-400 42%)	36.5
H-3	(-400 +450) 34% and (-400 42%)	37.5
H-4	(-400 +450) 34% and (-400 42%)	38.5
H-5	(-400) 34% and (-400) 42%	35.5
H-6	(-400) 34% and (-400) 42%	36.5
H-7	(-400) 34% and (-400) 42%	37.5
H-8	(-400) 34% and (-400) 42%	38.5

The blended powders were packed in tightly stoppered cylindrical rubber boots at a packing density of 3.5 gm/cm^3 and aligned in a 140 kOe field. These were cold isostatically pressed at $60,000 \text{ lb/in}^2$, removed from the rubber boots and packed into cylindrical thoroughly outgassed stainless steel cans. The stainless steel cans were then evacuated, baked out at 400°C , sealed under vacuum, and HIPped in a conventional hipping autoclave, where the hot isostatic pressing was carried out for two hours at 900°C under an argon pressure of $15,000 \text{ lb/in}^2$. Fig. 16

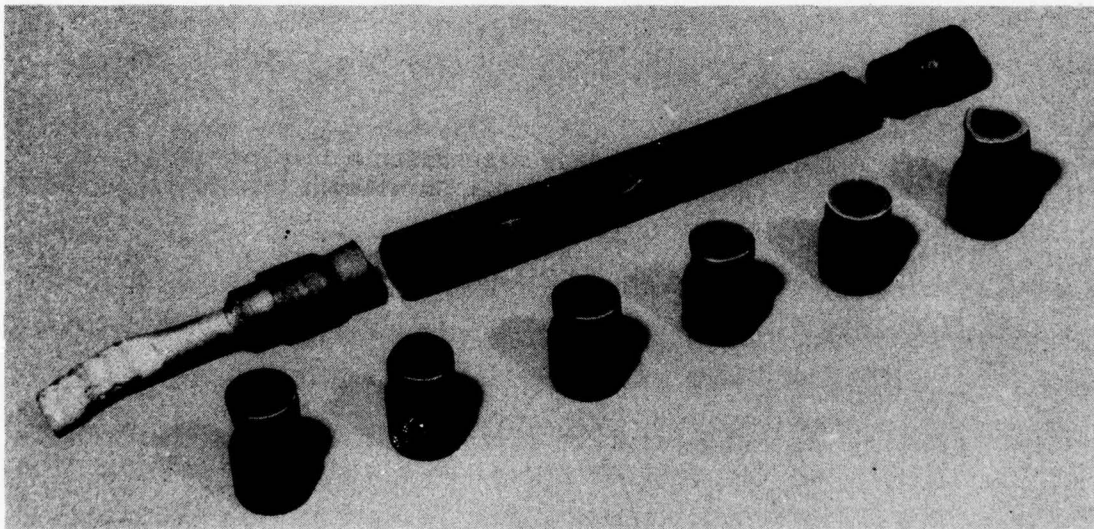


Figure 16. A HIPped magnet inside stainless steel container and polished end of a few others.

shows a hipped sample with its two ends sliced off by a diamond saw along with the ends of several others that were polished to reveal the microstructure of the samples. The end samples showed severe cracking of the Sm-Co alloys (see Fig. 17). However, slices cut further away from the ends showed very minimal cracking and good cylindrical samples have been produced by electro-discharge machining with the axis of the cylinder parallel to the original direction of magnetic axis. These cylindrical discs were used for (a) density measurements and (b) magnetic measurements, in as-HIPPed condition and after subsequent thermal optimization treatments.



Figure 17. Microphotograph of polished end of Sample H-7.

SECTION 9
RESULTS AND DISCUSSION

9.1 Powder Preparation

Particle size and size distribution of the powders prepared for HIPping and sintering have already been shown in Figs. 11 to 15. The significant features of these powders are their low oxygen content. The powders used in commercial magnets with an average particle size of about 10 μm contain anywhere from 0.5 to 1.0 weight percent oxygen. The commercially produced magnets contain one to two weight percent O_2 . With very careful attention to every step of the preparation, we have reduced the oxygen content of the powder by several fold (see Table 2).

Table 2. O_2 content at various stages.

Alloy		Weight Percent O_2
34%	As Received	0.04
	+325 mesh	0.064
	-325 mesh	0.221
	-400	0.215
	-400 +450 Used for HIPping	0.112
	Sinter powder: ground 25 minutes - attritor	0.128
42%	As Received	Not Determined
	+325 mesh	0.08
	-325 mesh	0.155
42%	-400 used for HIPping	0.108
	Sinter powder: ground 25 min. in attritor	0.251

A very substantial portion of the oxygen contamination from both the alloys was removed by rejecting the -325 mesh disc-pulverized material prior to fine grinding in the attritor. The oxygen level in the attritor ground product, which has much smaller particle size (one μm average) than the rejected -325 mesh pulverized product, is still very low. The oxygen pickup is only 0.064 weight percent in the case of 34 percent Sm alloy and 0.17 weight percent in the case of the 42 percent alloy over the +325 mesh powder. Most probably, the pickup occurred when the dried powder came in contact with air. However, we are extra careful in handling this powder. The blending operation is carried out under an argon cover to prevent further oxygen pickup.

9.2 Sintering

The initial sintering studies that we have performed so far were first, to check out the performance of the sinter furnace facility, and second, to determine (a) optimum composition, (b) proper sintering temperature and (c) optimization of heat treatment of sintered magnet. A few trial runs showed that the furnace produced very clean samples indicating that little if any contamination was introduced into the samples by the furnace treatment. The actual sinter runs were then made on each of the six compositions previously mentioned. The furnace was operated with vacuum in the muffle for temperatures up to 400°C and then switched over to flowing purified helium. In the first two runs the vacuum was maintained until the temperature reached 900°C. Since an excessive amount of Sm appeared to be evaporating off the samples during the first two runs, flowing gas was introduced into the furnace after a bake-out at 400°C in the subsequent runs, eliminating objectionable evaporation of Sm (reference Table 3).

Table 3. Sinter runs.

Run No.	Sinter Temperature °C	Gas Introduction Temperature °C	Sample Environment	Average Density Percent Theoretical	Porosity
1	1100	900	Open Tray in Helium	81.6*	Connected
2	1112	900	Open Tray in Helium	86.8*	Connected
3	1112	400	Open Tray in Helium	87.3*	Connected
4	1124	400	Open Tray in Helium	94.5	Isolated
5	1118	400	Open Tray in Helium	91.6	Isolated
6	1124	Not Introduced	Box with pumping holes and SmCo powder	88.6	Connected
7	1124	400	Box with pumping holes and SmCo powder	95.6	Isolated

No magnetic measurements were performed on runs No. 1 and 2 because of very low density. Measurement on run No. 6 sintered in vacuum, revealed them to be extremely poor magnetically. At this time we are not contemplating any more vacuum sintering. All samples of sinter runs 3, 4, 5, and 7 were measured and found to have enough potential. Following the measurement, they were annealed at 950°C for four hours, then quick-cooled and measured again. A second anneal of four hours at 900°C was given to the three lowest composition sample (36, 36.5, and 37 percent Sm) of these four sinter runs and remeasured. The measurements on runs 3, 4, 5 and 7 are given in Table 4.

Table 4. Measured magnet properties of sintered and heat treated samples.

Sinter Run No.	Alloy Mixture No.	Composition % Sm	Sinter Temp. °C	Percent Theoretical Density	Magnetic Properties After Sintering For 1 1/2 hours						Magnetic Properties After Anneal No. 1 4 hrs. - 950°C						Magnetic Properties After Anneal No. 2 4 hrs. - 900°C					
					B _r (kg)	H _c (kOe)	H _k (kOe)	H _{ci} (kOe)	BH (mGOe)	B _r (kg)	H _c (kOe)	H _k (kOe)	H _{ci} (kOe)	BH (mGOe)	B _r (kg)	H _c (kOe)	H _k (kOe)	H _{ci} (kOe)	BH (mGOe)			
3	1	36.0			6.05	6.0	19	26	9	6.75	6.65	12	38	12	6.55	6.55	29	37	11			
	2	36.5		Average	6.0	5.95	18	28	9	6.05	6.0	15	38	9	6.0	5.9	17	36	9			
	3	37.0	1112	87.3%	5.95	5.9	14	28	9	5.5	5.45	29	40	8	5.95	5.9	17	36	9			
	4	37.5		Porous	5.65	5.55	12	27	8	5.65	5.6	13	36	8								
	5	38.0			5.4	5.35	11	27	8	5.4	5.4	13	35	8								
	6	39.0			4.85	4.2	7	24	6	4.9	4.85	8	28	6								
5	1	36.0		91.2	7.1	7.05	18	23	13	7.1	7.0	17	40	13	7.05	7.0	21	42	12			
	2	36.5		91.5	6.95	6.8	15	25	12	6.9	6.8	12	37	12	6.85	6.8	17	40	12			
	3	37.0	1118	91.9	6.85	6.7	11	26	12	6.75	6.65	11	35	11	6.7	6.65	15	38	11			
	4	37.5		91.6	6.45	5.7	8	24	10	6.4	6.35	10	35	10								
	5	38.0		90.3						7.3	7.0	9	33	13								
	6	39.0		88.8						5.7	4.9	6	25	7								
4	1	36.0		93.0	7.25	7.15	17	25	13	7.36	7.25	15	38	14	7.25	7.2	19	40	13			
	2	36.5		94.9	7.25	7.2	12	22	13	7.35	7.2	10	31	13	7.25	7.25	15	35	13			
	3	37.0	1124 Open Tray	94.8	6.95	6.8	9	22	12	7.05	6.75	9	30	12	6.9	6.85	13	34	12			
	4	37.5		90.5	6.65	6.3	7	21	10	6.65	6.3	7	30	11								
	5	38.0		95.2	8.0	6.5	6	21	14	8.0	6.5	6	32	14								
	6	39.0		90.2	6.7	4.5	6	16	8	6.8	6.2	7	24	11								
7	1	36.0		94.8	7.5	6.35	4	15	12	7.5	7.4	19	36	14	7.45	7.25	16	37	13			
	2	36.5		95.6	7.45	7.35	11	19	14	7.4	7.2	11	30	14	7.4	7.3	14	32	14			
	3	37.0	1124 Box	95.6	7.25	6.8	9	19	13	7.2	7.0	9	28	13	7.15	7.1	13	32	13			
	4	37.5		95.5	6.95	6.4	7	19	12	6.9	6.55	8	25	12								
	5	38.0		95.3	6.7	5.35	6	19	9	6.7	6.25	7	28	11								
	6	39.0		91.9	5.95	4.15	3	18	7	5.9	5.4	6	25	9								

To clearly show the remarkable improvements in magnetic properties brought about by the low temperature anneals following the initial sintering, the second quadrant curves of a selected sample is shown in Fig. 18. In Fig. 19, the H_{ci} and H_k values are plotted against percent Sm for the magnets sintered at 1118°C . H_k is the reverse magnetic field at which 90 percent of the $4\pi M_r$ still remains, and as such, it is a measure of the stability of the magnets, and is therefore an important magnetic property. It appears that the magnets with composition between 36 and 37 percent are the best. We should therefore concentrate our efforts on them and also explore compositions with less than 36 percent Sm. A plot of H_{ci} versus sintering temperature for 36% Sm magnet in Fig. 20 shows high H_{ci} 's at lower temperatures. The limit on lower sintering temperature is set by the requirement of isolated porosity. The sintering temperature of 1112°C , although producing better magnetic properties, shows objectionable porosity and therefore is inferior to 1118°C sintering.

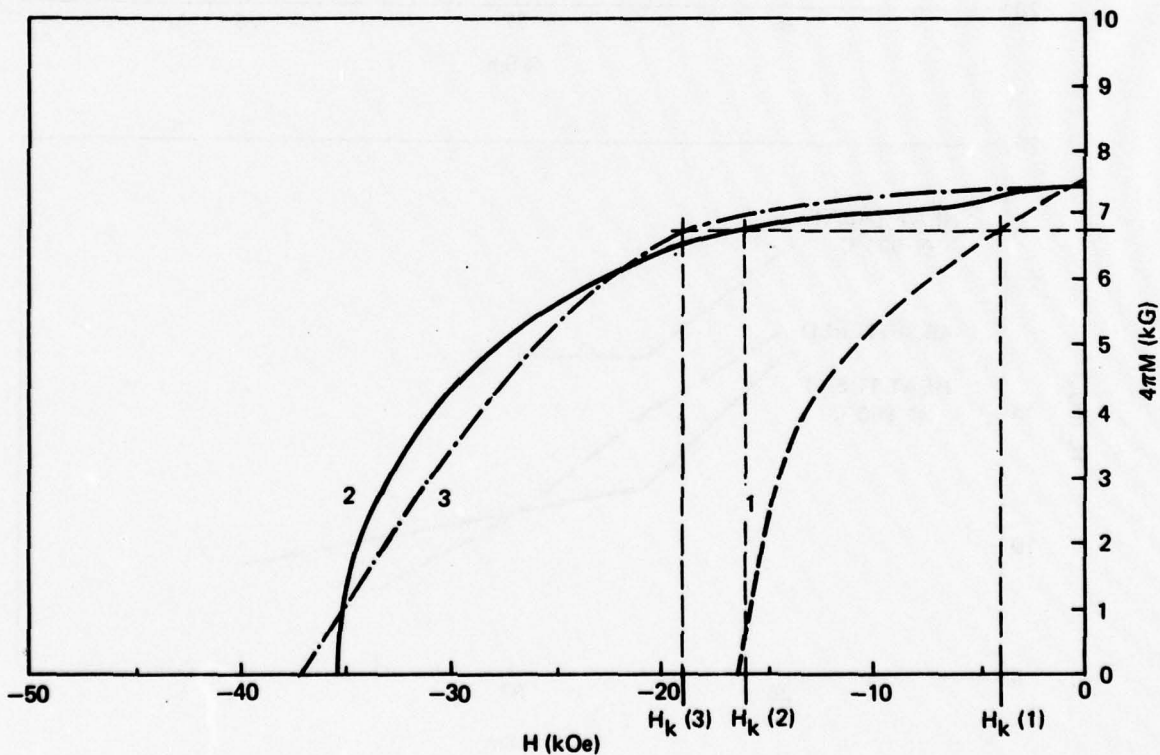


Figure 18. Demagnetization curves of sintered Sample No. 1 of sinter run No. 7. (1) as sintered, (2) after anneal No. 1 and (3) after anneal No. 2.

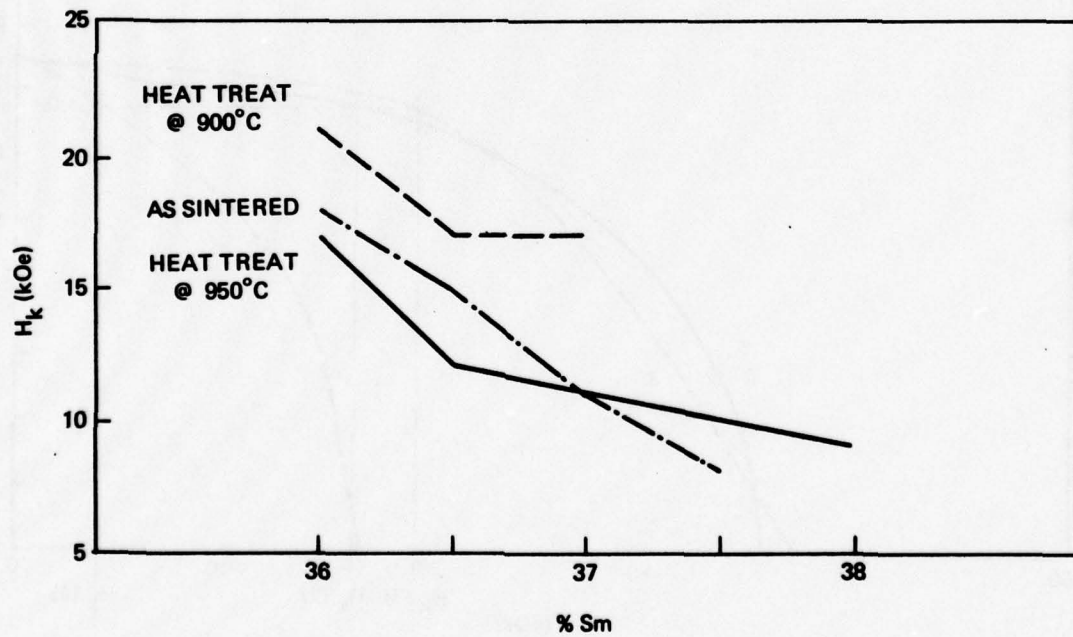
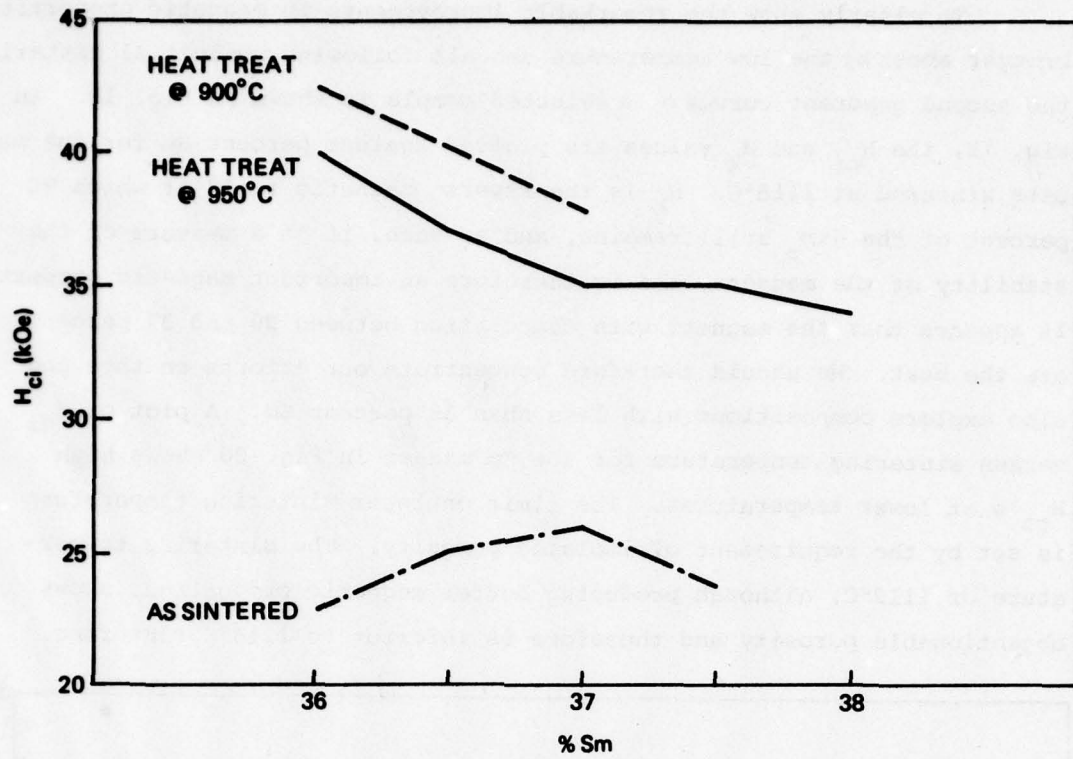


Figure 19. H_{ci} , H_k versus Sm content of samples sintered at 1118°C.

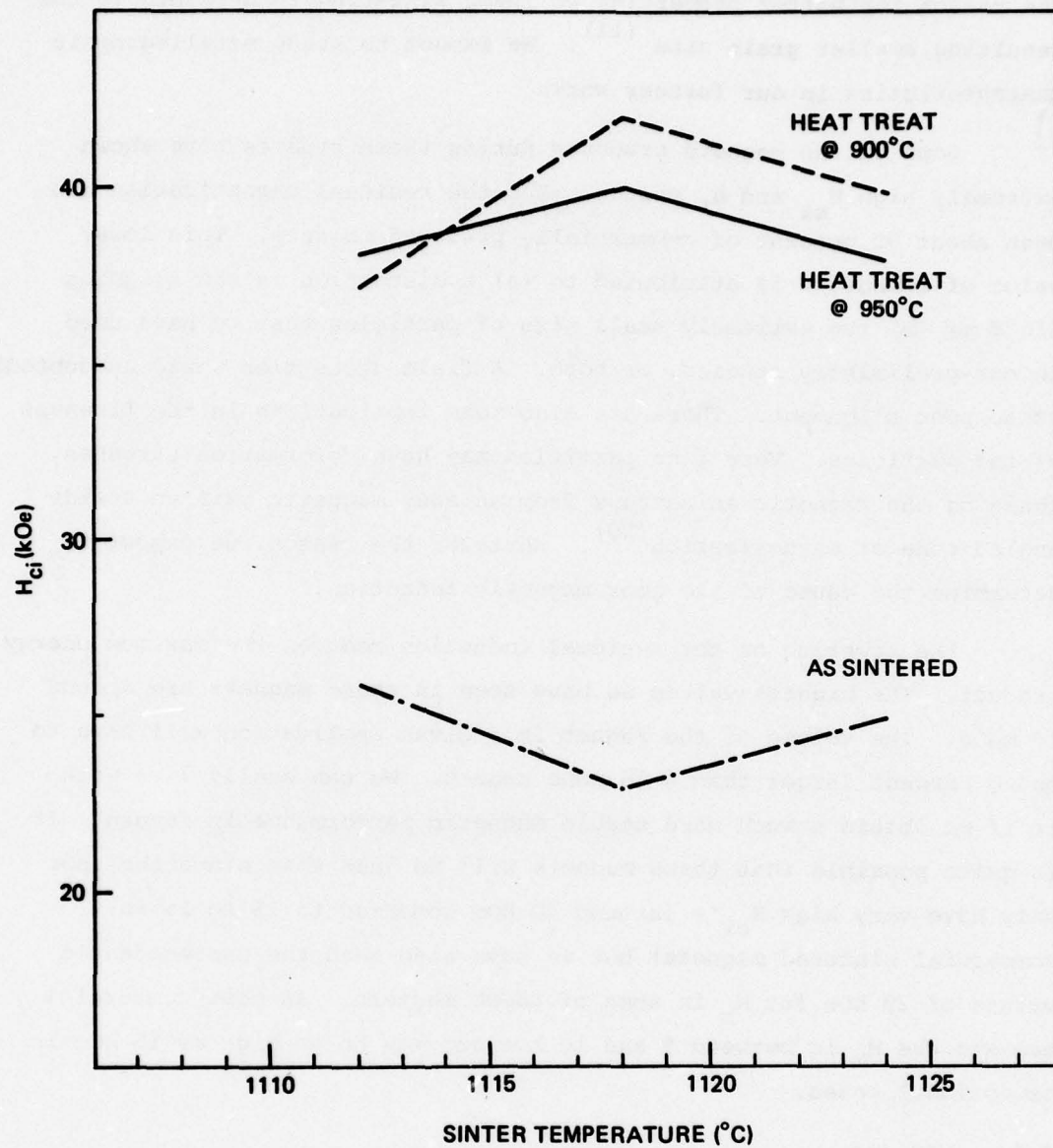


Figure 20. H_{ci} versus sinter temperature and effect of optimum anneals for alloy composition 36% Sm.

The reason for better properties at lower sintering temperature is the resulting smaller grain size ⁽¹¹⁾. We expect to study metallographic characteristics in our further work.

Some of the magnets produced during these studies have shown extremely high H_{ci} and H_k values. But the residual magnetization has been about 90 percent of commercially produced magnets. This lower value of remanence is attributed to (a) a distortion in the aligning field or (b) the extremely small size of particles that we have used in our preliminary studies, or both. A field distortion would undoubtedly cause poor alignment. There are also some implications in the fineness of the particles. Very fine particles may have deformation stresses, changing the magnetic anisotropy from an easy magnetic axis to a wide angled cone of magnetization ⁽²⁰⁾. Whatever the reason, we expect to determine the cause of the poor magnetic induction.

The lowering of the residual induction reduces the maximum energy product. The highest values we have seen in these magnets are around 13 mGOe. The volume of the magnet in a given application will have to be 20 percent larger than a 16 mGOe magnet. We can easily live with it if we obtain a much more stable magnetic performance in return. It is quite possible that these magnets will do just that since they not only have very high H_{ci} 's (around 40 kOe compared to 15 to 25 in commercial sintered magnets) but we have also seen the unprecedented values of 29 kOe for H_k in some of these magnets. In most commercial magnets the H_k is between 5 and 10 kOe but may be as high as 15 kOe in exceptional cases.

9.3 HIPping

Magnetic measurements were carried out on the spark machined samples in as-HIPped condition. The samples were then homogenized at 1000°C for 75 hours followed by quick cooling. A subsequent heat treatment of 900°C for four hours was given. Magnetic properties were measured after each of the above two heat treatments, the results of which are shown in Table 5.

Table 5. HIPped magnets.

Sample No.	Percent Sm	Percent Theoretical Density	Magnetic Properties As HIPped *					After First Heat Treatment 75 hrs. at 1000°C					After Second Heat Treatment 4 hrs. at 900°C				
			B _r	H _c	H _k	H _{ci}	BH	B _r	H _c	H _k	H _{ci}	BH	B _r	H _c	H _k	H _{ci}	BH
H-1	35.5	99.0	8.3	1.3	1.5	2.5	3	8.4	6.9	6	22	14	8.4	7.2	4	15	15
H-2	36.5	99.1	8.2	3	2.5	3	3	8.3	6.8	6	13	14	8.4	5.8	4	6	12
H-3	37.5	100	6.7	4.6	4	4	8	6.7	5.7	5	9	10	6.9	4.2	4	4	7
H-4	38.5	99.2	7.6	4	3	4	8	7.6	6.8	6	10	13	7.7	4.4	4	4	8
H-5	35.5	99.1	7.9	3.2	1.5	4	6	8.0	7.3	7	35	15	8.1	7.7	12	27	16
H-6	36.5	99.2	7.9	4.6	4	5	10	7.9	4.4	3	5	9	7.9	7.2	7	25	14
H-7	37.5	99.8	7.1	4.4	4	5	8	7.1	6.7	7	16	12	7.1	5.8	5	8	11
H-8	38.5	100	7.2	4.7	4	5	9	7.3	6.5	6	12	12	7.2	4.5	4	5	9

*B_r in kG, H_c, H_k and H_{ci} in kOe; and BH in mGoe

As expected, the densities of the HIPped samples are very close to the theoretical density. In Figs. 21 and 22, the microstructures of samples H-1 and H-5 are shown. It is quite evident that the porosities are very low. Sample H-5 shows smaller grain size than H-1, which is

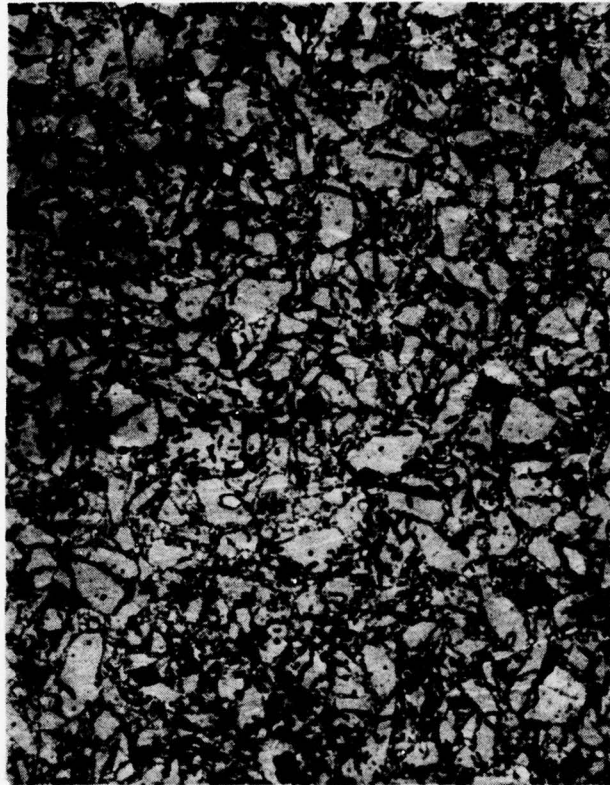


Figure 21. Microstructure of Sample H-1 in as-HIPped condition. 200X magnification.

consistent with the fact that samples H-1 through H-4 were prepared from coarser particle size (-400 +450) than H-5 through H-8 which had the base alloy powder size of -450 mesh. The powder size characteristics were maintained through the HIPping process and as a result the magnetic properties are better in the finer particle size group.

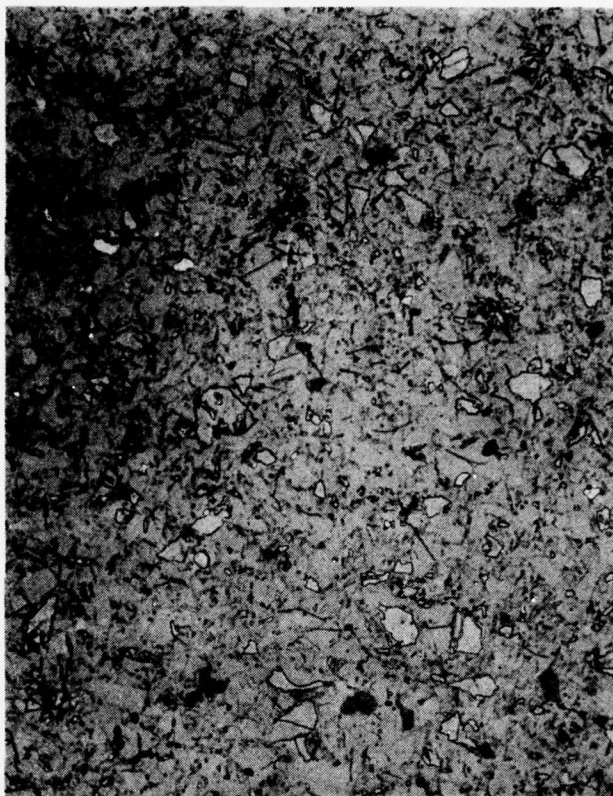


Figure 22. Microstructure of Sample H-5 in as-HIPped condition. 200X magnification.

The best composition was found to be the one having the lowest percentage of Sm - 35.5 weight percent. A plot of H_{ci} and H_k versus various thermal treatment temperatures for the samples H-1 and H-5, the best of the two groups, is shown in Fig. 23.

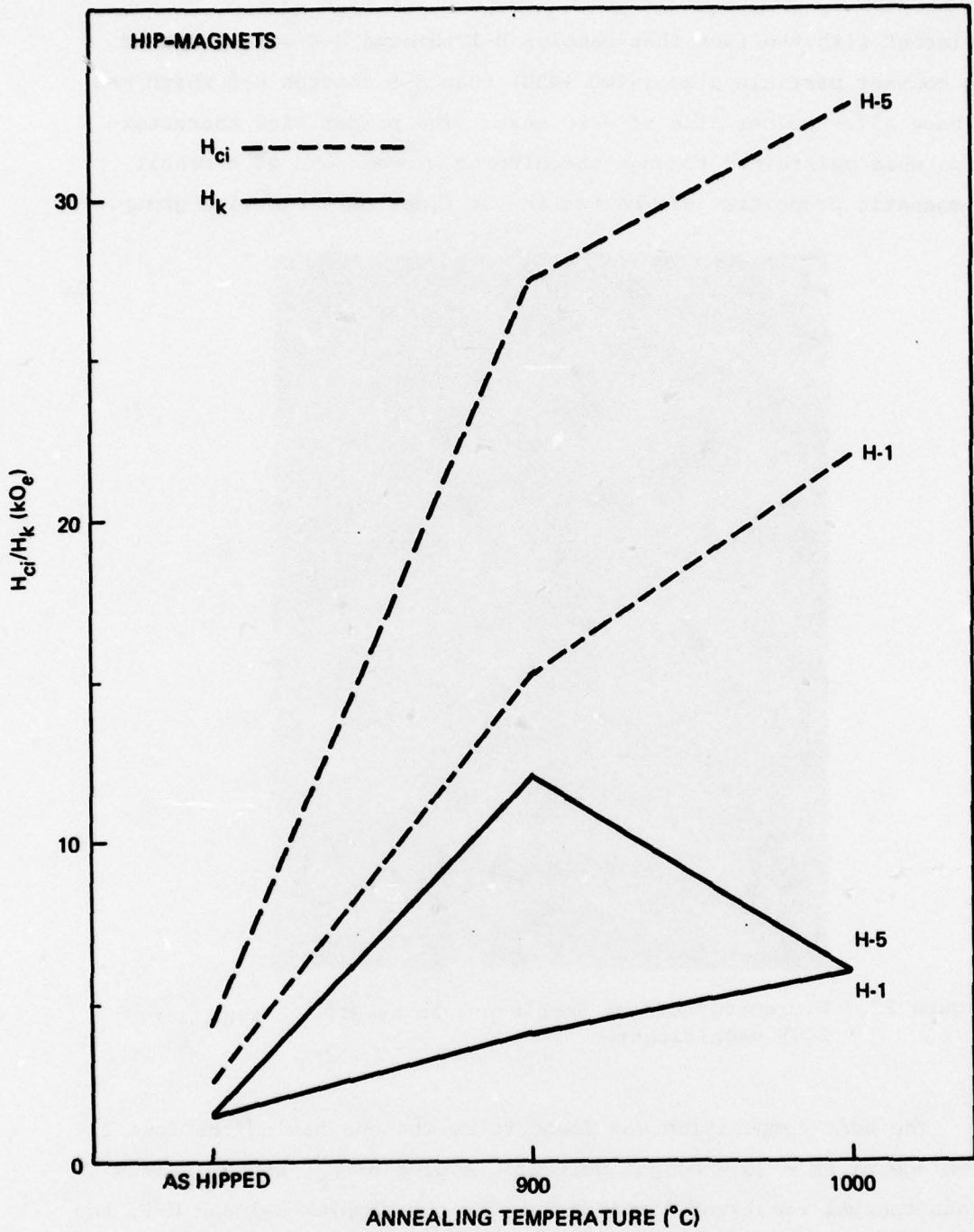


Figure 23. H_{ci} and H_k of HIPped Samples H-1 and H-5 in as-HIPped and annealed condition.

The properties of the as-HIPped samples are very poor, and are similar to the properties of the raw powders of the size used. However, the initial HIPping had done the two things we expected from the process, viz. it had produced (a) a nearly 100 percent dense body and (b) no grain growth. The next process of homogenization heat treatment of 75 hours at 1000°C brought about a remarkable improvement, and further improvement was shown by a shorter anneal of four hours at 900°C. Fig. 24 shows the above phenomena for sample H-5.

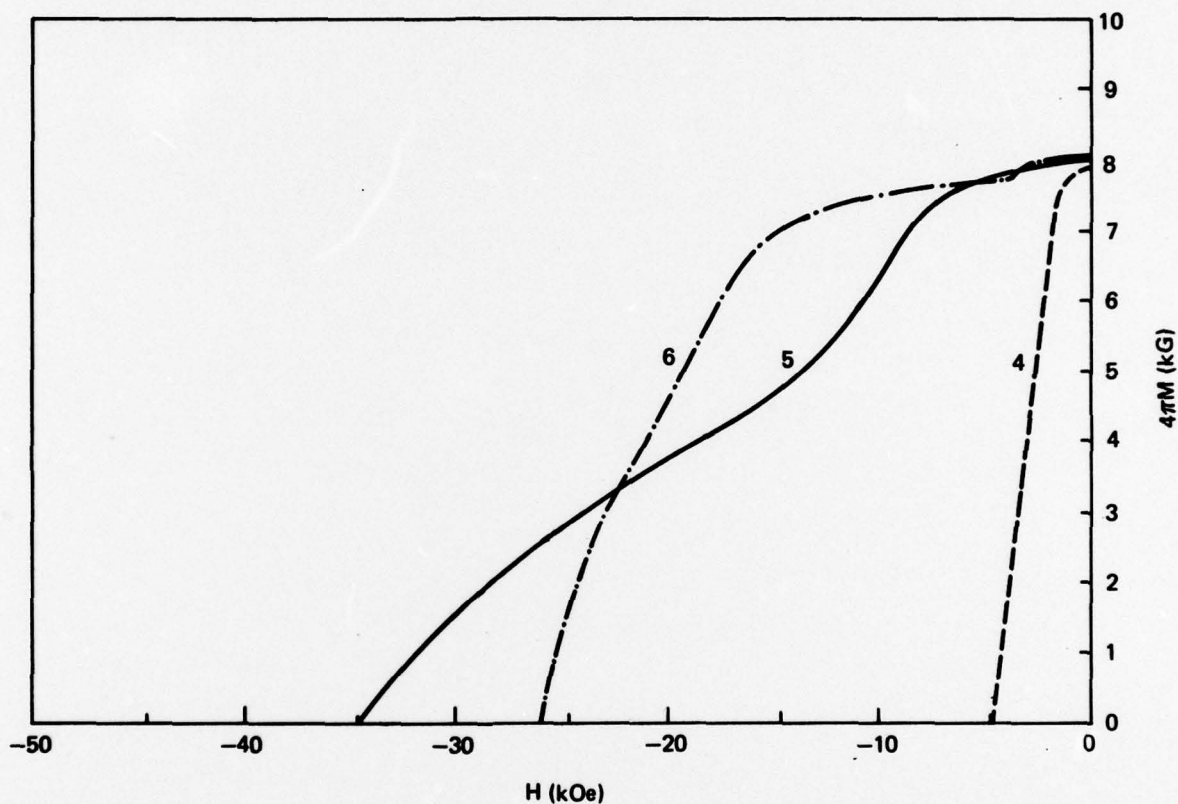


Figure 24. Demagnetization curves of HIPped Sample H-5. Curve (4) as HIPped, (5) after an anneal of 75 hours at 1000°C, and (6) further annealing at 900°C for 4 hours.

The results of the analysis...
...the...
...the...
...the...
...the...
...the...
...the...
...the...



blank
52

SECTION 10
CONCLUSIONS

10.1 Sinter Studies

Our initial sinter experiments have produced remarkable H_k values as high as 29 kOe compared to 5 to 10 kOe in normal sintered magnets. This has been possible because of the very high degree of success in the reduction of oxygen contamination in the preparation of powder of these alloys. As a result, we have been able to proceed with our sinter experiments with the average powder size of around 1.0 μm . This is about an order of magnitude smaller than in the present state-of-the-art fabrication process. It is possible that the superfine powder we have used has also contributed to a reduction of the energy product through unsatisfactory alignment capability. Even with the rather low energy product these magnets are expected to be very much more stable than commercial magnets and, as such, some stability measurements on these magnets are warranted. However, we are going to study and expect to determine the cause of misalignment.

10.2 HIPping Studies

The initial HIPping experiments have been extremely satisfying. The fact to remember is that we have used powder with the volume of average individual particles about 1000 times the volume of average particles in the usual sinter process. The reasons for using powder with such large particle size was to minimize the oxygen content and with the knowledge that there will be no further increase in grain size. As expected, our initial HIPping experiments have produced magnets comparable in quality to the best available commercially sintered magnets in spite of the large particle size. We expect outstanding results in future HIPping experiments using finer particle size.

We have come across two problems in our HIPping experiments, both related to the stainless steel container: (a) cracks in the magnet, and (b) difficulty of getting the magnet out of the container.

Cracks were believed to be caused by tensile stresses on the magnet core during cooling from HIPping temperature. The retention of very high mechanical strength by the container material is also a contributing factor.

The difficulty of removal of the container is associated with the low mechanical strength and brittle characteristics of the Sm-Co alloys. Machining-off of the stainless container was found impossible. Chemical dissolution of the stainless cover is just about impossible.

Based on the above reasoning, we will attempt our next HIPping experiments by replacing the stainless steel container with copper. Because of the low mechanical strength of copper, cracks are unlikely to occur. The container should be easily removable by dissolution in dilute nitric acid.

REFERENCES

1. Das, D., K. Kumar, and E. Wettstein, "High Stability Samarium-Cobalt Permanent Magnets," CSDL report C-4828, February 1977.
2. "Fabricating High Stability Sintered Sm-Co Magnets," Materials Research for Advanced Inertial Instrumentation, CSDL Proposal No. 7-780A, 1977.
3. Livingston, J.D., and M.D. McConnel, "Domain Wall Energy in Co-RE Compounds." J. App. Phys., Vol 43, No. 11, p. 4756, Nov. 1972.
4. Das, D. and W. Harrold, "Characterization of Sm-Co TWT Magnets," IEEE Trans., Mag-7, No. 2, p. 281, June 1971.
5. Mildrum, H.F., and K.M.D. Wong, "Stability and Temp. Cycling Behavior of R-Co Magnets," Proc. 2nd. Intnat'l Workshop on RE-Co Perm. Magnets, p. 35, June 1976.
6. Kumar, K., D. Das and E. Wettstein, "High Coercivity, Isotropic Plasma-Sprayed Sm-Co Magnets," J. App. Phys., Vol. 49, No. 3, Part II, p. 2052, March 1978.
7. Kumar, K., D. Das and E. Wettstein, "Sm-Co Magnets Resistant to 750°C," 16th Intermag Conf., Florence, Italy, May 1978.
8. Bartlett, R.W., and P.J. Jorgensen, "Microstructural Changes in SmCo₅ Caused by Oxygen Sinter-Annealing and Thermal Aging," J. Less Common Metals, 37, p. 21, 1974.
9. Das, D.K, et al, "Manufacturing Methods for Samarium-Cobalt Magnets," AFML TR-71-151, August 1971.

10. Benz, M.G., and D.L. Martin, "Cobalt-Mischmetal-Samarium Permanent Magnet Alloys, Process and Properties," J. App. Phys. 42, p. 2786, 1971.
11. Das, D.K., "Influence of Sintering Temperature on Magnetic Properties of Samarium-Cobalt Magnets," IEEE Trans. Mag., p. 432, Sept. 1971.
12. Becker, J.J., "Rare Earth Compound Permanent Magnets," J. App. Phys., 41, p. 10055, 1970.
13. Becker, J.J. "Permanent Magnets Based on Materials with High Crystal Anisotropy," IEEE Trans. Mag., Mag-4, p. 239, Sept. 1968.
14. Westendorp, F.F., "Nonaging Cold-Pressed SmCo_5 Magnets," IEEE Trans. Mag. 6, p. 472, 1970.
15. Tatsumoto, E., et al, "Saturation Magnetic Moment. . . High RCO_5 ," Jnl. de Physique, v. 32, p. CI-550, 1971 Supple.
16. Okamoto, T., et al, "Magnetic Moment and Easy Direction of Heavy Rare Earth Cobalt Compounds RCO_5 ," J. Phys. Soc., Japan, 34, p. 835, 1973.
17. Benz, M.G., R.P. Laforce, D.L. Martin, "A Co-Gd-Sm Permanent Magnet with a Zero Temperature Coefficient," AIP Conf. Proc., No. 18, p. 1173, 1974.
18. Jones, F.G., M. Tokunaga, "Low Temperature Coefficient Cobalt-Rare Earth Magnets," IEEE Trans., Magnetics, Vol. Mag-12, No. 6, p. 968, Nov. 1976.
19. Das, D. and K. Kumar, "New Technologies for Fabricating Improved Sm-Co Magnets," Proc. 3rd Intnat'l Workshop on R.E.-Co Magnets and Their Applications, Univ. of California, San Diego, California, June 1978.
20. Strnat, K., et al, "A Family of New Cobalt-Base Permanent Magnet Materials," J. App. Phys., Vol. 38, No. 3, P. 1001, March 1967.

BASIC DISTRIBUTION LIST

Technical and Summary Reports April 1978

<u>Organization</u>	<u>Copies</u>	<u>Organization</u>	<u>Copies</u>
Defense Documentation Center Cameron Station Alexandria, VA 22314	12	Naval Air Propulsion Test Center Trenton, NJ 08628 ATTN: Library	1
Office of Naval Research Department of the Navy 800 N. Quincy Street Arlington, VA 22217		Naval Construction Battalion Civil Engineering Laboratory Port Hueneme, CA 93043 ATTN: Materials Division	1
ATTN: Code 471	1	Naval Electronics Laboratory	
Code 102	1	San Diego, CA 92152	
Code 470	1	ATTN: Electron Materials Science Division	1
Commanding Officer Office of Naval Research Branch Office Building 114, Section D 666 Summer Street Boston, MA 02210	1	Naval Missile Center Materials Consultant Code 3312-1 Point Mugu, CA 92041	1
Commanding Officer Office of Naval Research Branch Office 536 South Clark Street Chicago, IL 60605	1	Commanding Officer Naval Surface Weapons Center White Oak Laboratory Silver Spring, MD 20910 ATTN: Library	1
Office of Naval Research San Francisco Area Office 760 Market Street, Room 447 San Francisco, CA 94102	1	David W. Taylor Naval Ship Research and Development Center Materials Department Annapolis, MD 21402	1
Naval Research Laboratory Washington, DC 20375		Naval Undersea Center San Diego, CA 92132 ATTN: Library	1
ATTN: Codes 6000	1	Naval Underwater System Center	
6100	1	Newport, RI 02840	
6300	1	ATTN: Library	1
6400	1	Naval Weapons Center	
2627	1	China Lake, CA 93555 ATTN: Library	1
Naval Air Development Center Code 302 Warminster, PA 18964 ATTN: Mr. F. S. Williams	1	Naval Postgraduate School Monterey, CA 93940 ATTN: Mechanical Engineering Department	1

BASIC DISTRIBUTION LIST (Continued)

<u>Organization</u>	<u>Copies</u>	<u>Organization</u>	<u>Copies</u>
Naval Air Systems Command Washington, DC 20360 ATTN: Codes 52031 52032	1	NASA Headquarters Washington, DC 20546 ATTN: Code RRM	1
Naval Sea System Command Washington, DC 20362 ATTN: Code 035	1	NASA (216) 433-4000 Lewis Research Center 21000 Brookpark Road Cleveland, OH 44135 ATTN: Library	1
Naval Facilities Engineering Command Alexandria, VA 22331 ATTN: Code 03	1	National Bureau of Standards Washington, DC 20234 ATTN: Metallurgy Division Inorganic Materials Division	1 1
Scientific Advisor Commandant of the Marine Corps Washington, DC 20380 ATTN: Code AX	1	Director Applied Physics Laboratory University of Washington 1013 Northeast Fortieth Street Seattle, WA 98105	1
Naval Ship Engineering Center Department of the Navy Washington, DC 20360 ATTN: Code 6101	1	Defense Metals and Ceramics Information Center Battelle Memorial Institute 505 King Avenue Columbus, OH 43201	1
Army Research Office P.O. Box 12211 Triangle Part, NC 27709 ATTN: Metallurgy and Ceramics Program	1	Metals and Ceramics Division Oak Ridge National Laboratory P.O. Box X Oak Ridge, TN 37380	1
Army Materials and Mechanics Research Center Watertown, MA 02172 ATTN: Research Programs Office	1	Los Alamos Scientific Laboratory P.O. Box 1663 Los Alamos, NM 87544 ATTN: Report Librarian	1
Air Force Office of Scientific Research Bldg. 410 Bolling Air Force Base Washington, D.C 20332 ATTN: Chemical Science Directorate Electronics and Solid State Sciences Directorate	1 1	Argonne National Laboratory Metallurgy Division P.O. Box 229 Lemont, IL 60439	1
Air Force Materials Laboratory Wright-Patterson AFB Dayton, OH 45433	1	Brookhaven National Laboratory Technical Information Division Upton, Long Island New York 11973 ATTN: Research Library	1

BASIC DISTRIBUTION LIST (Continued)

<u>Organization</u>	<u>Copies</u>	<u>Organization</u>	<u>Copies</u>
Library		Office of Naval Research	
Building 50, Room 134		Branch Office	
Lawrence Radiation Laboratory		1030 East Green Street	
Berkeley, CA	1	Pasadena, CA 91106	1

SUPPLEMENTARY DISTRIBUTION LIST

Technical and Summary Reports

Professor Albert E. Miller
University of Notre Dame
Box 8
Notre Dame, IN 46556

Professor Karl J. Strnat
University of Dayton
Magnetic Laboratory
Dayton, OH 45469

Dr. J. J. Becker
General Electric Research
and Development Center
P.O. Box 8
Schenectady, NY 12301

Professor W. E. Wallace
Department of Chemistry
University of Pittsburgh
Pittsburgh, PA 15213

Mr. A. E. Paladino
Raytheon Company, MPT Division
Waltham, MA

Dr. Richard P. Allen
Battelle-Northwest
Richland, WA 99352

Dr. Howard T. Savage
Naval Surface Weapons Center
White Oak
Silver Spring, MD 20910

Mr. Harold Garrett
Air Force Materials Laboratory
LTE, Bldg. 16
Wright-Patterson Air Force Base
Dayton, OH 45433

Dr. L. D. Jennings
Army Materials and Mechanics
Research Center
Watertown, MA 02172

Dr. J. O. Dimmock, Director
Electronic and Solid State
Sciences Program (Code 427)
Office of Naval Research
Arlington, VA 22217

Assistant Chief for Technology
(Code 2000)
Office of Naval Research
Arlington, VA 22217

Strategic Systems Projects Office
Department of the Navy
Washington, D.C.

Professor G. S. Ansell
Rensselaer Polytechnic Institute
Dept. of Metallurgical Engineering
Troy, NY 12181

Dr. David L. Martin
General Electric Research
and Development Center
P.O. Box 8
Schenectady, NY 12301

Professor M. Cohen
Massachusetts Institute of
Technology
Department of Metallurgy
Cambridge, MA 02139

Professor J. W. Morris, Jr.
University of California
College of Engineering
Berkeley, CA 94720

Professor O. D. Sherby
Stanford University
Materials Sciences Division
Stanford, CA 94300

SUPPLEMENTARY DISTRIBUTION LIST (Continued)

Dr. E. A. Starke, Jr.
Georgia Institute of Technology
School of Chemical Engineering
Atlanta, GA 30332

Professor David Turnbull
Harvard University
Division of Engineering and
Applied Physics
Cambridge, MA 02139

Dr. D. P. H. Hasselman
Montana Energy and MHD Research
and Development Institute
P.O. Box 3809
Butte, MT 59701

Dr. L. Hench
University of Florida
Ceramics Division
Gainesville, FL 32601

Dr. J. Ritter
University of Massachusetts
Department of Mechanical
Engineering
Amherst, MA 01002

Professor J. B. Cohen
Northwestern University
Dept. of Material Sciences
Evanston, IL 60201

Director
Materials Sciences
Defense Advanced Research
Projects Agency
1400 Wilson Boulevard
Arlington, VA 22209

Professor H. Conrad
University of Kentucky
Materials Department
Lexington, KY 40506

Dr. A. G. Evans
Dept. of Material Sciences
and Engineering
University of California
Berkeley, CA 94720

Professor H. Herman
State University of New York
Material Sciences Division
Stony Brook, NY 11794

Professor J. P. Hirth
Ohio State University
Metallurgical Engineering
Columbus, OH 43210

Professor R. M. Latanision
Massachusetts Institute of
Technology
77 Massachusetts Avenue
Room E19-702
Cambridge, MA 02139

Dr. Jeff Perkins
Naval Postgraduate School
Monterey, CA 93940

Dr. R. P. Wei
Lehigh University
Institute for Fracture and
Solid Mechanics
Bethlehem, PA 18015

Professor G. Sines
University of California
at Los Angeles
Los Angeles, CA 90024

Professor H. G. F. Wilsdorf
University of Virginia
Department of Materials Science
Charlottesville, VA 22903

SUPPLEMENTARY DISTRIBUTION LIST (Continued)

Dr. F. Rothwarf (DELET-ES)
Dept. of the Army
HQ, U.S. Army Electronic Command
Fort Monmouth, NY 07703

Dr. D. T. Stevenson
National Magnet Laboratory
Massachusetts Institute of
Technology